Physics – Uspekhi **63** (5) 417 – 439 (2020)

REVIEWS OF TOPICAL PROBLEMS PACS numbers: 02.70.Ns, **64.10.+h**, 64.70.D–

Complex phase diagrams of systems with isotropic potentials: results of computer simulations

V N Ryzhov, E E Tareyeva, Yu D Fomin, E N Tsiok

DOI: https://doi.org/10.3367/UFNe.2018.04.038417

Contents

Abstract. This review is based on a talk by the authors at the field Scientific session of the Physical Sciences Division of the Russian Academy of Sciences devoted to the 60th anniversary of the Vereshchagin Institute for High Pressure Physics of the Russian Academy of Sciences. The dependence of phase-diagram characteristics and phase transitions on the shape of the intermolecular potential is reviewed and analyzed for two- and three-dimensional systems with isotropic interaction. First, the case of monotonic repulsive and attractive parts of the potential is considered. In particular, it is demonstrated that if the width of the attractive part decreases, the critical point can disappear and even go under the melting curve. In the main part of the review, three-dimensional systems with potentials having a negative curvature in the repulsive region, that is, with two spatial scales in this region, are discussed in detail: in this case, a number of crystalline phases can occur, as can maxima on the melting curve, water-like anomalies, and liquid–liquid transitions. The dependence of the melting scenario on the shape of the potential in two-dimensional systems is also discussed.

V N Ryzhov [(1)], **E E Tareyeva** [(2)], **Yu D Fomin** [(3)], **E N Tsiok** [(4)]
Vereshchagin Institute for High Pressure Physics,
Russian Academy of Sciences,
Kaluzhskoe shosse 14, 108840 Troitsk, Moscow, Russian Federation
E-mail: [(1)] ryzhov@hppi.troitsk.ru, [(2)] eetare@gmail.com,
[(3)] fomin314@mail.ru, [(4)] elena.tsiok@gmail.com

Received 15 August 2018, revised 6 December 2019
Uspekhi Fizicheskikh Nauk **190** (5) 449 – 473 (2020)
Translated by E N Ragozin; edited by A M Semikhatov

Keywords: theory of liquids, effective potential, core-softened potential, liquid anomaly, structural anomaly, diffusion anomaly, density anomaly, two-dimensional system, melting scenario, Berezinskii–Kosterlitz–Thouless–Halperin–Nelson–Young theory, Hertz potential, phase diagram

1. Introduction

This review [1] is concerned with an important and dynamically developing modern area of condensed matter physics dealing with so-called soft matter, including solutions of proteins, polymers, colloids, and dust plasma. In contrast to inert gases, whose phase diagram is known to be simple and can be described with a high accuracy using well-known isotropic effective Lennard-Jones-type potentials, a much more complex phase behavior is observed in a number of systems, for instance, liquid metals or water. In such systems, the interaction is described by complex anisotropic potentials, which in principle can be estimated by rather arduous ab initio simulations. This brings up the question: can a family of pairwise isotropic potentials be generalized so as to describe, at least at a qualitative level, the observed complicated phase behavior, including numerous crystal phases, maxima on the melting curves, thermodynamic and dynamic water-like anomalies, liquid–liquid-type transitions, as well as different melting scenarios in the two-dimensional case? For this, we consider the effect of the shape of the intermolecular potential

[1] This review is based on the talk given on behalf of the authors by Yu D Fomin at the anniversary Scientific Session of the Physical Sciences Division of the Russian Academy of Sciences (RAS) dedicated to the 60th anniversary of the Vereshchagin Institute for High Pressure Physics (HPPI) (see Refs [1–3]).

on the structure of the phase diagram and the phase transitions in two- or three-dimensional systems described by this potential.

The simplest pairwise potential is the hard-sphere potential

$$U(r) = \begin{cases} \infty, & r \leqslant d, \\ 0, & r > d, \end{cases} \tag{1}$$

where d is the sphere diameter. The hard-sphere system was the first to come under the scrutiny of the molecular dynamics method [4–7]. Simulations of a hard-sphere system showed that with increasing pressure it undergoes a transition from a disordered phase to a face-centered cubic (fcc) crystal. From potential (1), it is clear that the potential energy of the system is always equal to zero. The melting curve of the system is therefore of the form $\rho_\mathrm{l} = \text{const}$ and $\rho_\mathrm{c} = \text{const}$, where ρ is the density ($\rho = N/V$, with N particles in a volume V), and ρ_l and ρ_c are the liquid and crystal densities on the phase coexistence line. In the three-dimensional description of systems with a hard core, the packing density $\eta = (\pi/6)\rho d^3$ is typically used instead of the density ρ. For hard spheres, the melting curve parameters are $\eta_\mathrm{l} = 0.494$ and $\eta_\mathrm{c} = 0.545$. At a higher density, a stable crystal phase exists up to $\eta \approx 0.74$, corresponding to close-packed fcc or hexagonal close-packed (hcp) lattices [8]. In the pressure–temperature plane, the melting curve of hard spheres is defined by the relation [9, 10]

$$P = \frac{c'}{d^3} T, \tag{2}$$

where $c' \approx 12$ is the proportionality coefficient, which can be estimated in different ways: by computer simulations [120] or from the equation of state for hard spheres in Carnahan–Starling or Percus–Yevick approximations [8, 11]. Therefore, in a system of hard spheres, the phase equilibrium line is a straight line emanating from the origin. As follows from the form of the free energy $F = (3/2)NkT - TS$ for a system of hard spheres, the phase transition in this system is controlled exclusively by the entropic part of the free energy. As shown by computer simulations in Ref. [12], the entropy of even a slightly supercooled liquid of hard spheres is always lower than that of a crystal of the same volume and temperature (see Fig. 8 in Ref. [13]). The crystal phase of hard spheres at sufficiently high densities has a higher entropy than the liquid phase, because there is more free space for fluctuations about equilibrium positions in the crystal; self-organization into a crystal structure is entropic in nature [9, 10, 13].

The behavior simplicity of a system of hard spheres, as well as the existence of an exact analytic solution in the Percus–Yevick approximation, which describes the structure and the equation of state of the liquid phase for hard spheres, makes this system attractive for use as the initial system in the construction of a perturbation theory describing the behavior of more complex systems [14]. In particular, the density functional method in the theory of crystallization, which is based on the theory of inhomogeneous liquids, relies on precisely this system as the initial approximation [11, 16, 17, 231].

Despite its simplicity, the system of hard spheres provides a suitable description of several experimental facts. In particular, it was shown in Ref. [18] that the structural factors of liquid metals are nicely approximated by the structural factors of effective hard spheres. In particular, the packing densities of effective hard spheres were recently calculated [19] on the melting curve of iron. It turns out that these packing densities coincide with the packing density on the melting curve of hard spheres. This testifies to the fact that the melting of metals is determined primarily by the repulsive potential core.

A natural generalization of the hard-sphere potential is the soft-sphere potential

$$U(r) = \varepsilon \left(\frac{\sigma}{r} \right)^n, \tag{3}$$

where ε, σ, and n are the model parameters. The thermodynamic behavior of the model exhibits scaling properties [9, 23]: the properties of a system of soft spheres can be described in terms of the universal reduced quantity $\gamma = \rho\sigma^3 (k_\mathrm{B} T/\varepsilon)^{-3/n}$, where k_B is the Boltzmann constant and T is the temperature (the Klein theorem [9, 20–23]). The Klein theorem permits obtaining scaling relations for the behavior of thermodynamic quantities along the melting line [9, 22, 23]. The model is useful in the investigation of the role of repulsion in crystallization. The dependence of crystal structure on the softness of the potential was studied by computer simulations [24, 25]. The system was shown to crystallize into a close-packed fcc structure for $n > 6.25$, while the body-centered cubic (bcc) structure was shown to be stable for softer potentials.

Similar results were also obtained for the Yukawa potential $U(r) = \varepsilon \exp(-\kappa r)/r$, where $1/\kappa$ is said to be the range of the force. As shown by computer simulation methods in Refs [26–29] (see also Ref. [30]), for large κ (short-range potentials), the system crystallizes into an fcc structure, while a bcc lattice appears in the opposite case of a long-range potential. At intermediate values of κ, both phases exist with a first-order transition between them [29, 30].

As first shown by van der Waals in his famous equation, the attraction between molecules underlies the existence of the gas–liquid transition. As an example, we consider a system with the Lennard-Jones potential

$$U(r) = 4\varepsilon \left[\left(\frac{\sigma}{r} \right)^{12} - \left(\frac{\sigma}{r} \right)^{6} \right]. \tag{4}$$

The parameter σ defines the spatial scale and ε defines the energy scale in the system. Figure 1 schematically shows the phase diagram of the system with the Lennard-Jones potential. It contains the gas, liquid, and crystal existence domains, as well as the two-phase domains between them. The phase diagram shows the triple T_t and critical T_cr points. As is clear from Fig. 1, the liquid phase exists in the temperature interval $T_\mathrm{t} < T < T_\mathrm{cr}$. The critical point exists due to precisely the attractive part of the potential. The presence of the liquid phase in the phase diagram is critically dependent on the shape of the attractive part of the potential: a variation in the depth of the attractive part does not change the phase diagram structure qualitatively, but merely results in a temperature renormalization in the phase diagram. However, a variation in the width of the attractive part can result in a radical restructuring of the phase diagram. This problem has been the subject of active studies [30–33] by computer simulations for model potentials: systems of hard spheres with the addition of an attractive part in the form of the Yukawa potential [31] or a rectangular attractive well [32, 33]. The liquid phase was shown to be stable when the width

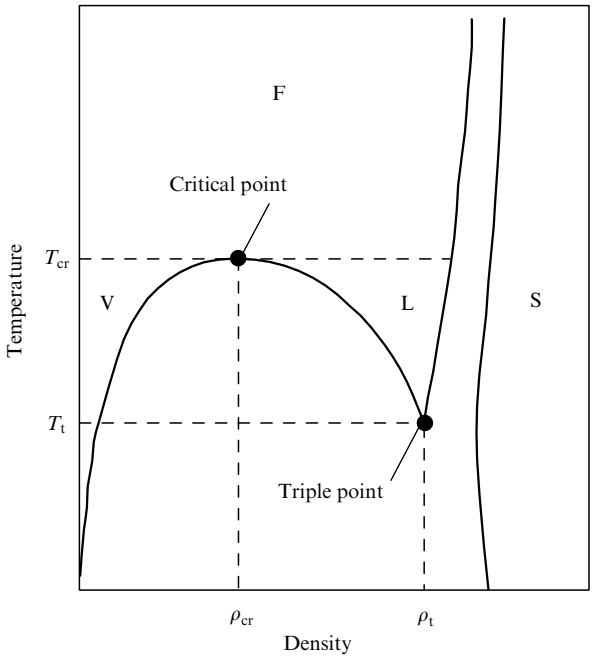

Figure 1. Phase diagram of a system with Lennard-Jones potential (4) (see Ref. [11]).

of the attractive part of the potential was about 15–20% of the diameter of the hard-core potential.

We note that the application of the Lennard-Jones potential to the description of real systems, first of all, rare gases, results in serious errors at high pressures and temperatures. The reason may be that the many-particle interactions should not be disregarded under these conditions. However, it is possible to obtain sufficiently reliable results by using the Buckingham potential (or exp (−6) [34]) parameterized for use at high pressures and temperatures [35–37]. This potential is characterized by a softer repulsion at short range compared with the Lennard-Jones potential and can be written as [35]

$$U_B(r) = \varepsilon\left\{\frac{6}{\alpha-6}\exp\left[\left(1-\frac{r}{r^*}\right)\right]-\frac{6}{\alpha-6}\left(\frac{r^*}{r}\right)^6\right\}, \quad (5)$$

where ε, α, and r^* are fitting parameters. The qualitative phase diagram for potential (5) is similar to that shown in Fig. 1.

In colloidal suspensions, the width of the attractive part can be changed by varying the experimental conditions. For instance, the width of the attractive potential in a colloid–polymer mixture can be changed by increasing or decreasing the density and the relative size of the colloids and polymers [38]. Investigations of the behavior of different colloidal systems, both theoretical and experimental, suggest that a critical point exists at which the width of the attractive part of the potential exceeds 15% of the hard-core diameter [30, 40–42, 78, 139].

In connection with the existence problem of a critical point, we note a system with the Girifalco potential [44] proposed to describe the efficient interaction between the C_{60} fullerene molecules. Qualitatively, the shape of the Girifalco potential resembles the shape of Lennard-Jones potential (4) (although the analytic formula is more complex), but the relative width of the attractive part is much smaller. Monte Carlo simulations [45] suggest that a stable liquid phase is absent and the sublimation line passes above the metastable gas–liquid transition domain [30, 45]. But the situation is somewhat controversial: as shown in Refs [46–48] using the method of molecular dynamics, the liquid phase does nevertheless exist in the system, although in an extremely narrow temperature interval. By and large, it is valid to say that narrowing the relative width of the attractive part is indeed responsible for the disappearance or, at least, for the narrowing of the existence domain of the stable liquid phase. It is commonly stated that the system exists in a homogeneous state above the critical temperature (supercritical region). At the same time, according to very recent investigations, in the supercritical region we are dealing with two special lines: the Widom line and the Frenkel line. The former was proposed in Ref. [49] as the line of correlation length maxima above the critical point (the correlation length diverges in approaching the critical point). Based on the assumption that the generalized susceptibilities of the system (heat capacity, thermal expansion coefficient, compressibility) are proportional to the correlation length in the vicinity of the critical point, it was suggested to consider this line as the continuation of the gas–liquid or liquid–liquid transition curve, which divides the supercritical region into gas-like and liquid-like domains (see, e.g., Refs [52, 96, 97]). At the same time, we showed in [53–57] that this definition does not apply to the above division because the maxima of thermodynamic quantities decay quite rapidly with the distance from the critical point. Furthermore, the maxima of different thermodynamic quantities form a 'fan' of lines that coincide with the line of the correlation function maximum only in the immediate vicinity of the critical point and rapidly diverge from each other with the distance from this point. In this case, their mutual arrangement depends on the thermodynamic path along which they can be approached. However, the gas-like and liquid-like states do exist at temperatures well above the melting line, including in the supercritical region. As shown in our work by computer simulations as well as in several experiments, these domains are separated by a dynamic crossover line at which transverse excitations in the liquid vanish at any frequency available in the system. This line was termed the Frenkel line in honor of the Soviet scientist Yakov Frenkel, who made a major contribution to liquid state physics. We note that there are several other criteria related, for instance, to the behavior of the velocity autocorrelation function, to the heat capacity at constant volume, as well as to local structure variation and positive sound dispersion [57–72]. Unlike the Widom line, which exists only in systems with a critical gas–liquid transition point, the Frenkel line also exists in systems with a purely repulsive soft-sphere potential (3). Detailed discussion of the supercritical behavior and the Frenkel line is beyond the scope of this review and can be found in the cited literature and review [73].

The evolution of the phase diagram of a colloidal system as the width of the potential is varied is shown schematically in Fig. 2, which was borrowed from [74]. A similar phase diagram can be obtained, for instance, for the double Yukawa potential [75, 76] $U(r) = \varepsilon/r\,[\exp(-a(r-1)) - \exp(-b(r-1))]$, $a > b$, in the framework of the van der Waals theory adapted to describe solids [75–77]. By varying the parameters a and b, it is possible to change the width of the potential without changing its depth. Figure 2a shows a standard phase diagram (see Fig. 1) corresponding to the attractive part of the potential of a sufficiently large width. Shown below the

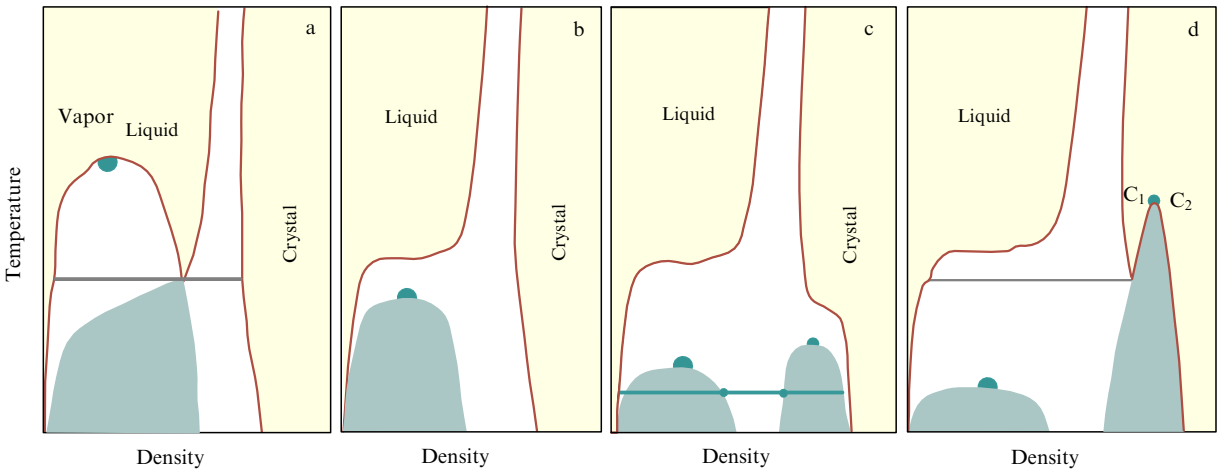

Figure 2. (Color online.) Evolution of the phase diagram under narrowing the attractive part of the potential (see Refs [74, 78]). (a) Standard phase diagram corresponding to a sufficiently wide attractive part of the potential. Shown below the triple point temperature is the metastable region of direct gas–solid transition (of sublimation). (b) Phase diagram of a system with short-range attraction (less than 15% of the hard-core diameter). In this case, the critical point of the gas–liquid transition shifts to the metastable domain below the melting point. (c) Phase diagram for an even narrower part of the attractive potential (2% of the hard core). In the metastable domain below the melting point, apart from the gas–liquid critical point at low density, an isostructural transition appears between two solid phases of high density. (d) Phase diagram of a system with an extremely narrow attractive part of the potential with a stable isostructural transition between two crystal phases C_1 and C_2.

temperature of the triple point is the metastable domain of the direct gas–solid transition (of sublimation). Figure 2b corresponds to short-range attraction (less than 15% of the hard-core diameter). In this case, the critical point of the gas–liquid transition shifts to the metastable domain below the melting point. In the case of an even narrower part of the attractive potential (2% of the hard core diameter), in the metastable domain below the melting point, apart from the gas–liquid critical point at low density, an isostructural transition appears between two solid phases at high density. As the attractive part of the potential is made even narrower, a stable isostructural transition appears between two crystal phases C_1 and C_2 [45]. As recently shown in Ref. [79], in the case of an isostructural transition, there is also a Widom line, analogous to the Widom line for the gas–liquid transition, with similar properties.

Although the above models made it possible to describe the formation mechanism of the main phase transitions, melting and boiling, they do not give rise to numerous other effects typical of many real systems. The interaction in real systems is described by complex anisotropic potentials (for instance, for water and silicon). In some cases, however, the properties of these systems can be validly described by well-known isotropic effective potentials like the Lennard-Jones potential. At the same time, it is commonly known that several systems, like liquid metals and water, exhibit a much more complex phase behavior than simple systems (for instance, rare gases) typically do and cannot be described by simple standard potentials. This brings up the question: can the family of isotropic potentials be generalized so as to describe the observed anomalous behavior? We discuss this problem in the following sections of this review.

A variety of liquids with anomalous properties different from 'normal' liquids like argon have been discovered experimentally. The best-known representative of these systems is water, in which more than 70 anomalies have been discovered (see, e.g., Ref. [80]). In particular, while normal liquids contract under isobaric cooling, water expands at temperatures below 4 °C at atmospheric pressure. Similar behavior has been observed experimentally, for instance, in Te, S, P, Se, GeTe, SeTe [81–87, 95, 102, 109–112] and observed in computer simulations for SiO_2, S, and BeF_2 [80, 90–94]. All these systems have a highest-density temperature: below this temperature, the coefficient of thermal expansion at constant pressure becomes negative. In the literature, this is referred to as the density anomaly.

At the same time, water exhibits anomalous behavior also in several other aspects, for instance, in the dynamics and structure. While the diffusion coefficient of normal liquids decreases with increasing density or pressure, there is a phase diagram domain for water where diffusion is enhanced as the pressure increases. As shown experimentally, at a temperature of 283 K, the normal behavior of water sets in only at pressures above 1.1 kbar [88].

Normal liquids tend to become more ordered under compression. In computer simulations, this is usually characterized by an increase in the integral of the radial distribution function, which is erroneously termed the order parameter in some papers and is defined as [174, 177, 178]

$$\tau = \frac{1}{\xi_c}\int_0^{\xi_c} \left|g(\xi) - 1\right| \mathrm{d}\xi\,, \tag{6}$$

where $\xi = r\rho^{1/3}$ is the interparticle distance r normalized to the average interparticle distance $\rho^{-1/3}$, $g(\xi)$ is the radial distribution function, and ξ_c is the truncation length, which is usually taken equal to half the side of the box that confines the system being modeled. In an ideal gas, $g(r) = 1$ and $\tau = 0$. In a normal liquid, the degree of ordering increases with density, and this is attended by an increase in τ, which testifies to an increase in translation order. However, as shown in the framework of molecular dynamics [88, 178], in water there is a phase diagram domain in which this parameter decreases as the density or pressure increases at a constant temperature. A similar behavior was discovered in computer simulations of silica [91].

Interestingly, these anomalies in water follow a sequence that was comprehensively determined both experimentally and by computer simulations: in the temperature–density plane, the structural anomaly domain completely encompasses the diffusion anomaly domain, which in turn contains the density anomaly [88, 178]. However, in other liquids, this sequence can be different. For silica, for instance, the diffusion anomaly domain contains the structural anomaly domain, which in turn surrounds the density anomaly domain [91].

Another anomaly that has been attracting considerable recent attention is the possible liquid–liquid transition in a one-component system in addition to the standard gas–liquid critical point. The possible coexistence of two liquid phases, the low-density liquid (LDL) and the high-density liquid (HDL), was first discovered in selenium Se in 1989 [95]. For water, a similar behavior was predicted on the basis of computer simulations in 1992 [81, 88, 98]. By that time, it was well known that water has two amorphous phases: the low-density amorphous (LDA) and high-density amorphous (HDA) phases separated by a sharp crossover line, which has the character of a first-order transition [81, 96, 97]. Discovered in 2001 was one more amorphous state of water, which is more dense than the HDA [88, 99–101]. This property, termed polyamorphism, i.e., the existence of more than one amorphous state, is usually related to polymorphism — the existence of more than one crystal phase of the same substance. A typical example of a polymorphous substance is water, which has at least 16 forms of ice. Experimental data compatible with the notions of liquid–liquid and amorphous-phase–amorphous-phase transitions were obtained for silicon, selenium, and cobalt, as well as for quasi-two-dimensional and quasi-one-dimensional water in nanopores [81, 103–107]. Similar behavior was observed in cerium-based metallic glasses [108]. The critical point of the liquid–liquid transition was predicted in the framework of computer simulations for different models of water, phosphorus, silicon, etc. [81, 88, 89, 93, 98]. It is pertinent to note that direct in situ experimental observations of the transition between a low-density molecular liquid and a high-density polymer liquid were made only in phosphorus [73, 81, 109–111] and maybe in sulfur [112]. The transition in phosphorus is attended by significant structural changes and a sharp density step (of the order of 30%), which is unambiguously interpreted as a first-order transition.

In 1970, Hemmer and Stell [113] (see also Refs [114, 115]) proposed the model of a potential with a negative curvature of its repulsive part (a core-softened potential). The negative curvature of the potential has the effect that an inflection point appears on the repulsive part of the potential, giving rise to two characteristic scale lengths in the system. One of them corresponds to the hard core of the potential and the other to the distance of the inflection point from the origin. As shown below, owing to the appearance of several characteristic length parameters in the potential, the system can form several structures characterized by different interparticle distances. The simplest example of such a potential is the hard-sphere potential with a repulsive step added to it:

$$U(r) = \begin{cases} \infty\,, & r \leqslant \sigma\,, \\ \varepsilon\,, & \sigma < r \leqslant \sigma'\,, \\ 0\,, & r > \sigma'\,, \end{cases} \tag{7}$$

where σ is the diameter of the hard core, σ' is the repulsive step width, and ε is its height.

S M Stishov suggested calling potential (7) the potential of 'collapsing hard spheres'. A qualitative analysis of the phase diagram of this system was done in Ref. [116] (see also Refs [117–119]) and is presented in Fig. 3. As is clear from Eqn (7), in the low-temperature limit $\tilde{T} \equiv k_{\mathrm{B}}T/\varepsilon \ll 1$, the system reduces to hard spheres of diameter σ', while in the limit $\tilde{T} \gg 1$ the system is equivalent to hard spheres of diameter σ. We revert to Eqn (2) to conclude that the melting curve at low and high temperatures can be written in a single form $P = cT/\sigma''^3$, where $c \approx 12$ and σ'' is the diameter of the corresponding hard sphere (σ or σ') [120]. The crossover from the low-temperature to high-temperature behavior of the melting curve of the system of collapsing spheres occurs for $\tilde{T} = \mathcal{O}(1)$. The exact form of the phase diagram depends on the ratio $s \equiv \sigma'/\sigma$. For instance, a maximum in the melting curve would be expected to appear for sufficiently large s (see Fig. 3), while the maximum should vanish in the limit $s \to 1$ [116]. In the temperature domain $\tilde{T} = \mathcal{O}(1)$, we can expect a complex behavior of the system, including not only maxima in the melting curve but also different crystal phases [121–123] and a liquid–liquid transition [117–119, 124–128]. On the strength of the aforesaid, in the crossover region, the system can be regarded as an effective mixture of particles with diameters σ or σ'. Therefore, the system behaves like a binary mixture of particles of different diameters, the concentration of particles of each sort depending on the temperature and density. In the subsequent discussion, such systems are termed quasibinary.

Following the work of Hemmer and Stell, many different models with core-softened potentials have appeared (see, e.g., Refs [129–137]). For example, we mention the following potentials under active investigation:

$$U(r) = 4\varepsilon\left[\left(\frac{\sigma}{r}\right)^{12} - \left(\frac{\sigma}{r}\right)^{6}\right] + a\varepsilon \exp\left[-\frac{1}{c^2}\left(\frac{r - r_0}{\sigma}\right)^2\right], \tag{8}$$

where a, c, and r_0 are parameters of the potential [130], and a potential of the form

$$U(r) = \frac{U_R}{1 + \exp\left(\Delta(r - R_R)/a\right)} - U_A \exp\left[-\frac{(r - R_A)^2}{2\delta^2}\right] + \left(\frac{a}{r}\right)^{24}, \tag{9}$$

with parameters a, U_R, Δ, δ, R_R, and R_A [131, 132].

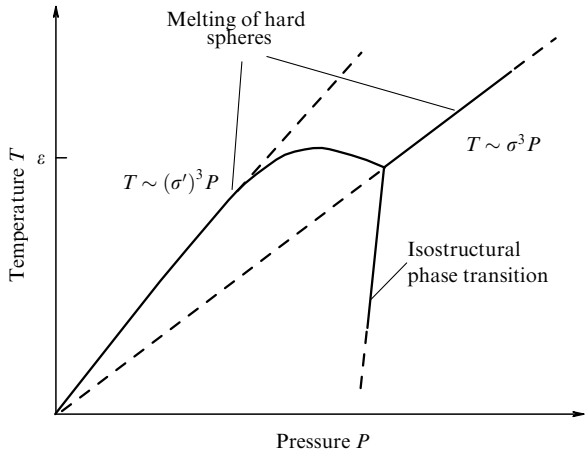

Figure 3. Phase diagram of a system of collapsing hard spheres [10, 116].

We also mention the potentials corresponding to deformable particles (colloids, polymer globules, star-shaped polymers, etc. [138]). One such potential is the Hertz potential [139, 158], whose properties are discussed at greater length in Section 5.2. In particular, systems with this potential exhibit anomalous behavior three and two dimensions [158, 140, 252, 253]. Another potential under active study, which is suited to describe highly deformable particles and is regular at the origin, is the Gaussian potential [141, 142] of the form

$$U_{\mathrm{GCM}} = \varepsilon \exp\left[-\left(\frac{r}{\sigma}\right)^2\right]. \tag{10}$$

The systems described by potential (10) (or its modifications with the addition of a Gaussian attractive part) exhibit a number of unusual properties, including water-like anomalies and complex phase diagrams with maxima and minima in the melting curves [143–149, 158]. Studying these models yielded a qualitative description of several important phenomena in phase transitions: the appearance of a maximum on the melting curve, the formation of complex structures that had previously been observed only in systems with anisotropic potentials, for instance diamond structures, liquid–liquid transitions, etc. Furthermore, studying systems with core-softened potentials made it possible to shed light on the emergence of anomalous behavior of liquids, which had hitherto been largely attributed to complex many-particle and anisotropic particle interactions in liquids.

A remark is in order here. As shown in Refs [151–153] in the framework of the mode coupling theory [166], the system of collapsing hard spheres allows describing not only the liquid–glass transition but also glass–glass transitions between two different vitreous states.

2. Three-dimensional systems with core-softened potentials. Potential of smoothed collapsing spheres

Our initial aim was to use computer simulations to investigate the behavior of a system with a collapsing sphere potential for different parameter values of the potential. However, to simplify the application of molecular dynamics techniques to this system, we proposed a smoothed potential of the form [154–157]

$$\frac{U(r)}{\varepsilon} = \left(\frac{\sigma}{r}\right)^{14} + \frac{1}{2}\left(1 - \tanh\left(k\left(r - \sigma_1\right)\right)\right). \tag{11}$$

The parameters σ and ε define the length and energy scales. These parameters can be used to construct the system of units associated with the potential: $\tilde{r} = r/\sigma$, $\tilde{T} = k_{\mathrm{B}}T/\varepsilon$ (k_{B} is the Boltzmann constant), etc. We use these dimensionless units in what follows. Because only dimensionless units are used in what follows we, omit the tildas.

Figure 4 depicts the shape of potential (11) for several σ_1 values. We can see that this potential consists of a hard core, which has a power-law divergence at zero, and a smoothed step. The parameter σ_1 defines the width of the repulsive step. In what follows, this potential is referred to as the potential of smoothed collapsing spheres (SCSs). (We note that more recently this potential was 'rediscovered' and presented under the name 'Fermi–Jagla potential' in Ref. [159]; see also, e.g., Ref. [160].)

A simple criterion of the possibility of anomalous behavior of a system was proposed by Debenedetti et al. [150]. The criterion is based on the consideration of the behavior of the thermal expansion coefficient as a function of the parameters of the core-softened potential. It can be shown that according to the Debenedetti criterion, anomalous behavior is expected for potential (11) if $\sigma_1 > 1.16$.

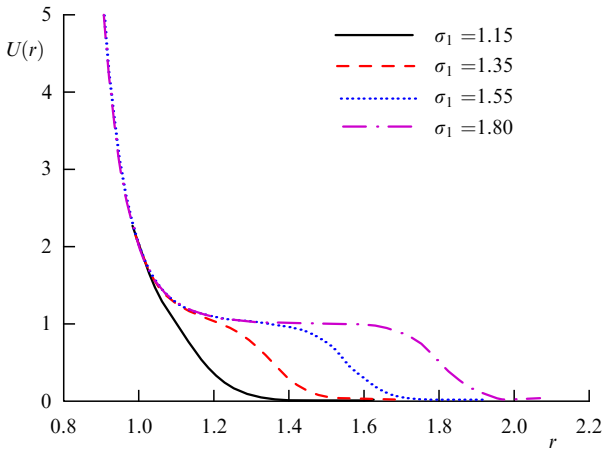

Figure 4. (Color online.) Potential of smoothed collapsing spheres for several values of the parameter σ_1.

The evolution of a system described by potential (11) is analyzed in relation to the width of the repulsive step. We calculated the phase diagrams and thermodynamic properties of the system of SCSs for the step widths $\sigma_1 = 1.15, 1.35, 1.55$, and 1.8. The first of the σ_1 values is slightly less than the critical value obtained from the Debenedetti criterion. The phase diagram of the system of smoothed collapsing spheres was first published in our paper [154]. Subsequent publications [155–157] have supplemented this paper by clarifying the results obtained and adding the phase diagrams for other potential parameter values.

The first paper [154] (see also Ref. [155]) studied the behavior of the system of smoothed collapsing spheres with the following parameter values defining the step width: $\sigma_1 = 1.15$, 1.35, and 1.55. The phase diagram of the system with $\sigma_1 = 1.35$ was complemented in subsequent study [157]. The phase diagram of the system with $\sigma_1 = 1.8$ was presented in Ref. [156].

The phase diagrams and thermodynamic properties of the systems were studied by computer simulations using the Monte Carlo and molecular dynamics methods. These methods are well known and are expounded, e.g., in book [161]. In calculating the phase diagrams, the following approach was used. At the first stage, possible crystal structures were constructed: we selected several structures typical of the systems under consideration, in particular, those with core-softened potentials, and calculated their energies as functions of the density at zero temperature. After that, the structures most stable in a given density range were modeled by the Monte Carlo method at a finite temperature to obtain an approximate estimate of the stability domain for one crystal phase or another. However, this method of estimating the melting curves is very coarse, and the phase diagrams obtained by such simulations cannot be considered exact. Therefore, in the final derivation of the lines of coexistence of different phases, we calculated their Helmholtz free energies by the method of thermodynamic integration [161]. The equilibrium transition densities were

calculated by constructing the common tangent to the free energies of coexisting phases as functions of the volume. The transition pressure was obtained from the slope of the common tangent. In this case, the abscissas of the tangency points determine the volumes of coexisting phases (in our case, they are solid and liquid phases) [162]. In this way, it is possible to construct the complete phase diagram of the system, including the coexistence domains. A disadvantage of this approach is that the crystal phase structure does not result from the evolution of the system in a natural way: it is set 'manually'. Selected in this case is a minimal-energy structure at given thermodynamic parameters. This is precisely the circumstance that accounts for the appearance of 'gaps' in the phase diagrams shown below, which may contain complex crystal structures with large unit cell volumes not observed in the simulations.

To construct a phase diagram, including the phase coexistence domain at a first-order phase transition, we can also use the calculation of the equation of state, which then exhibits van der Waals loops (also termed Mayer–Wood loops in the case of two dimensions). By the well-known Maxwell construction, it is possible to determine the phase boundaries and the two-phase domain. This approach is especially convenient in two dimensions (see Section 5), when calculating the Helmholtz free energy is difficult.

2.1 Potential with step $\sigma_1 = 1.15$

We begin by addressing the phase diagrams of smoothed collapsing spheres with the smallest repulsive step among those under consideration: $\sigma_1 = 1.15$. This step is so narrow that in reality the potential is strongly different from 'true' collapsing spheres and is close to the soft-sphere potential $U_{\text{soft}} = \varepsilon(\sigma/r)^{14}$. Furthermore, this potential does not satisfy the Debenedetti criterion, i.e., strictly speaking, it is not a core-softened potential. We recall that only one crystal phase, fcc, can exist for soft spheres with the softness index $n = 14$ [163].

Despite the superficial similarity of the potential under study and soft spheres, the phase diagram of the system is significantly different. Three crystal domains appear in the system: a low-density fcc phase and high-density bcc and fcc phases (Figs 5a and 5b).

The system of soft spheres with a softness index $n < 6.25$ is known to crystallize into the bcc phase, while the system with a higher index does so into the fcc phase [25]. That is why the existence of the fcc–bcc–fcc sequence in the system under study is an indication that the effective softness of the potential decreases in the domain of the bcc phase stability.

Similar results were obtained in Ref. [164]. These authors studied a system of 'true' collapsing spheres, which was defined by Eqn (7), using perturbation theory methods for several step widths. For the step $\sigma_1 = 1.16$, they obtained a qualitatively similar phase diagram with the fcc–bcc–fcc transition sequence.

2.2 Potentials with steps $\sigma_1 = 1.35$ and $\sigma_1 = 1.55$. Analogy with behavior of quasibinary systems

As the step is increased to $\sigma_1 = 1.35$, the potential begins to satisfy the Debenedetti criterion. This has the effect that the phase diagram becomes more complex.

We consider the qualitative behavior of the system with $\sigma_1 = 1.35$. We begin with the study of system structure variation along the low-temperature isotherm $T = 0.1$. Figure 6a shows the radial distribution functions (RDFs) of the system for low densities and Fig. 6b shows the RDFs for

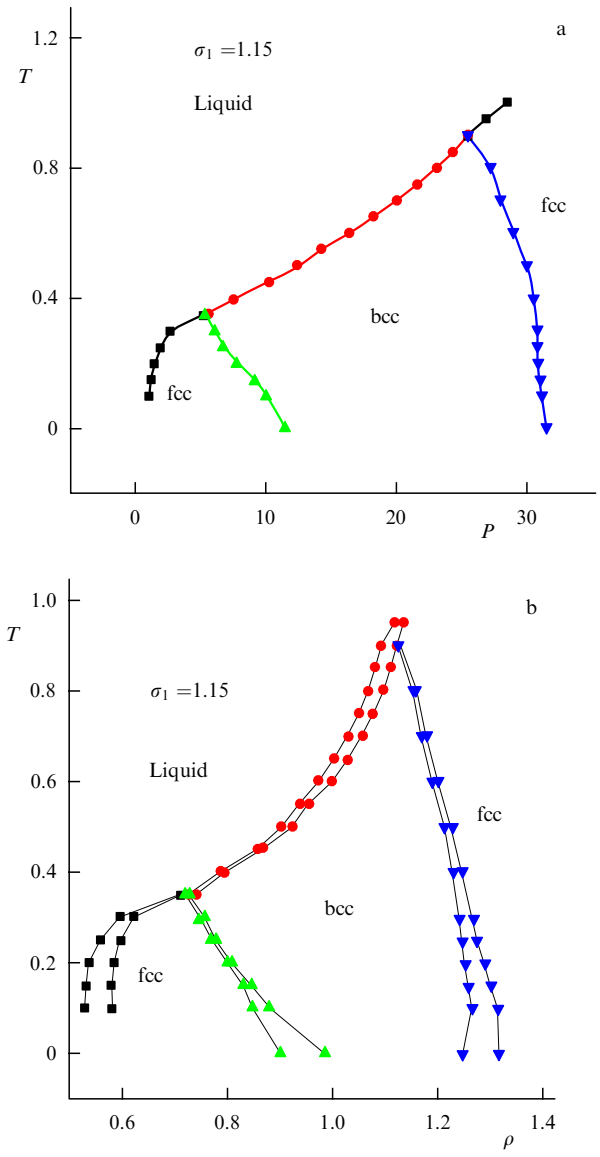

Figure 5. (Color online.) Phase diagram in (a) $P-T$ and (b) $\rho-T$ coordinates for the step $\sigma_1 = 1.15$.

high densities. As can be seen from Fig. 6a, for the density $\rho = 0.3$ the RDF has the form typical of a liquid. The first peak is located at a distance of about 1.5, which is somewhat longer than the step width $\sigma_1 = 1.35$. We recall that the first RDF peak is typically located at a distance somewhat longer than the effective particle size. Therefore, at this density, it is valid to say that $\sigma_1 = 1.35$ is the effective size of the atoms. As the density increases to $\rho = 0.4$, the RDF assumes a typical crystalline form. It follows from calculations of the distances to the ith neighbors and the corresponding coordination numbers that this is an fcc crystal with the lattice constant $a = 1.5$. However, a subsequent increase in density gives rise to a new disordered structure for $\rho = 0.5$. A characteristic RDF feature for $\rho = 0.5$ is the existence of two peaks at the distances $r = 1.1$ and $r = 1.5$. At lower densities, the peak at $r = 1.1$ is not observed. Hence, it follows that increasing the density from 0.4 to 0.5 leads to a significant change in the local structure of the system, associated with a closer particle approach to each other, or 'collapse' in Stishov's terminology [116]. Under a further increase in density, the system

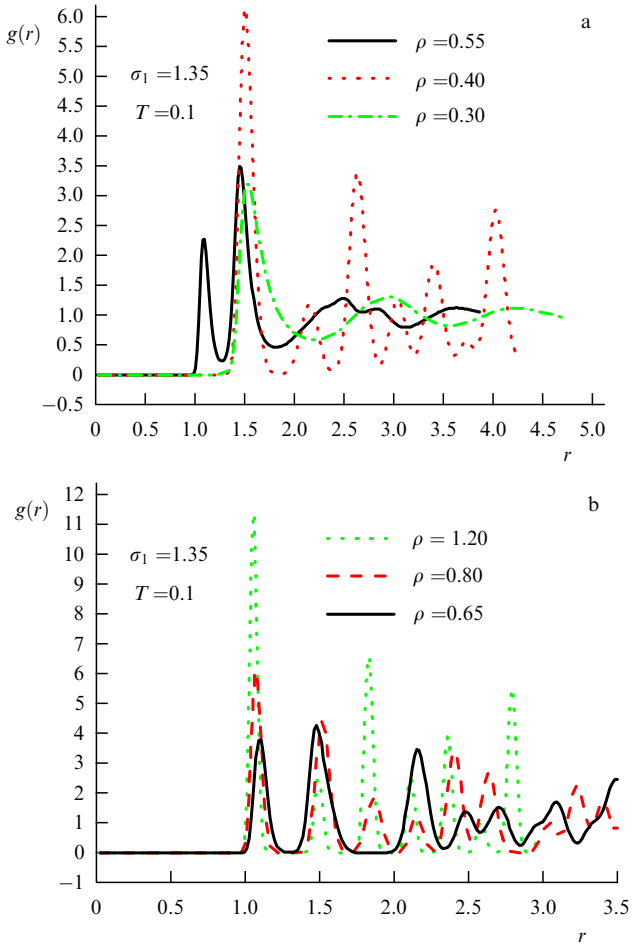

Figure 6. (Color online.) Radial distribution functions of the system with the $\sigma_1 = 1.35$ step along the $T = 0.1$ isotherm for various density values.

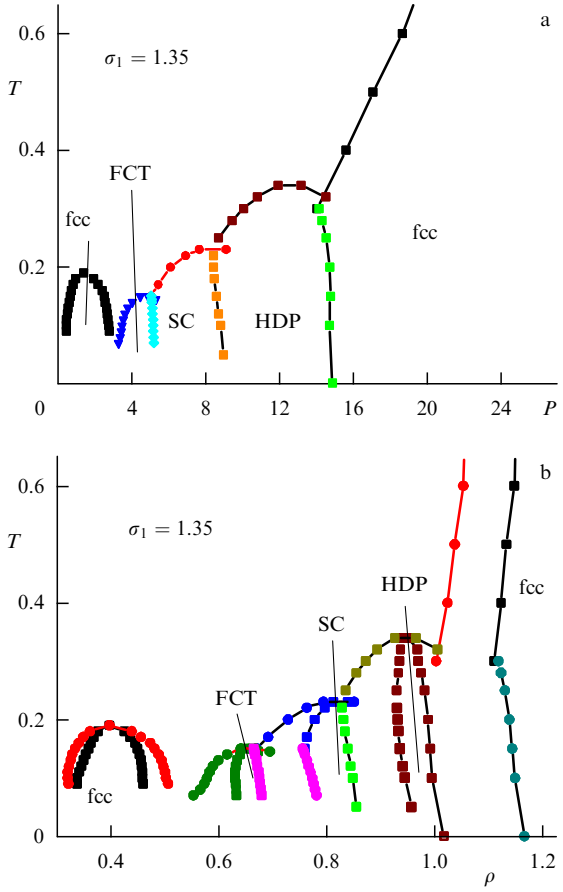

Figure 7. (Color online.) Phase diagram in (a) $P-T$ and (b) $\rho-T$ coordinates for the step $\sigma_1 = 1.35$.

crystallizes once again, but into different phases. As is clear from Fig. 6b, for $\rho = 0.65$, the $r = 1.0$ and $r = 1.5$ peaks become practically equal in height. As the density increases further, the height of the first peak increases rapidly. As this takes place, there is a change in the configuration of the peaks: the characteristic distances between them and the relative heights. This indicates a change of the crystal structures in the system.

As mentioned above, the maximum of the first peak for particles of size σ is at a distance somewhat longer than σ. We can see from Figs 6a and 6b that the effective particle size at low densities is determined by the step width σ_1. As the density increases, initially a peak appears at a distance equal to the potential core σ, and then this peak begins to grow to become equal in height to the one located at the distance equal to the step width. Therefore, two characteristic scale lengths appear in the system. The existence of two characteristic scale lengths is typical of binary systems, i.e., when there are particles of two types. In the system under consideration, there are particles of one type, and we are therefore dealing with a quasibinary-type system. Under a further density increase, the peak located at the distance σ defined by the potential core becomes prevalent, i.e., at a high density the effective particle size is determined just by the potential core. We note that this behavior of the system is in qualitative agreement with the picture proposed by Stishov in Ref. [116] (see Fig. 3).

Figure 7 shows the phase diagram of the system in the density–temperature and pressure–temperature coordinates. We can see that it consists of two low- and high-density fcc phases and several phases between them. This form of the phase diagram is intuitively clear. Because the potential is purely repulsive, the particles tend to minimize the overlaps both of 'hard' cores and of steps. Therefore, for relatively low densities, crystallization of the system occurs into a low-density fcc phase, which corresponds to the dense packing of the particles spaced at the step width. With increasing density, the particles begin to approach each other at distances shorter than the step width, and disordering occurs. The subsequent increase in density results in crystallization of the system. However, to minimize the number of overlaps, the system crystallizes into loose structures, whose coordination number increases with density: a face-centered tetragonal (fct) lattice with 4 nearest neighbors, a simple cubic (sc) with 6, and an hcp with 12. In the high-density limit, the system crystallizes into the high-density fcc phase.

We note that there is a domain in the phase diagram of this system in which we did not find a stable crystal phase. This domain corresponds to the densities between the low-density fcc structure and the fct phase. As discussed above, the system under discussion exhibits the property of quasi-binarity, which manifests itself in the existence of two characteristic scale lengths in the one-component system. By quasibinarity we mean the following property: under specific

conditions, which depend on thermodynamic parameters, the system can be treated as a mixture of two types of particles with different hard-core diameters. Phase diagrams of binary systems are typically more complex than those of single-component substances. Complex structures with a large number of particles in the elementary cell can emerge in binary mixtures. We can expect that extremely complex structures undetectable by the methods in use can also occur in the case of the quasibinary system being studied. Therefore, the system effectively behaves like a binary mixture. Many binary systems can undergo a transition to glass. Preliminary simulations performed in Ref. [154] suggest that the system does undergo a transition to glass. More recently, these simulations were confirmed by more careful simulations in Ref. [167]. We also mention Ref. [168], where the possible existence of a dodecagonal quasicrystal in the system with the potential of smoothed collapsing spheres (11) with $\sigma_1 = 1.37$ was shown. This reaffirms the high sensitivity of the shape of phase diagrams to the parameters of the potential.

The behavior of a system with the step $\sigma_1 = 1.55$ is similar to the previous case $\sigma_1 = 1.35$. Also observed in this case is a low-density fcc phase, which melts with increasing density, i.e., the effect of reentrant melting occurs. By reentrant melting we mean an effect due to which a system initially crystallizes and then melts again as the density increases at constant temperature. This effect corresponds to the phase diagram with a maximum on the melting curve. However, the sequence of crystal phases emerging after the 'reentrant' liquid phase is different from the previous case: simple cubic, hexagonal, intermediate-density fcc, bcc, high-density fcc. We note that this system also exhibits a 'gap' in the phase diagram, in which no stable crystal phase was discovered. As in the previous case, we believe that this 'gap' accommodates some complex crystal structure, which is impossible to detect by the methods in use, or glass.

Increasing σ_1 to 1.8 complicates the phase diagram still further [156]. In particular, two gaps appear in the phase diagram as do several new crystal phases, but the behavior of the system remains qualitatively the same.

3. Phase diagram of a system of smoothed collapsing spheres with attraction

In the preceding section, we considered the phase diagrams of a system of smoothed collapsing spheres. As is evident from the results outlined, varying the step width has a significant effect on the phase diagram of the system. The aim of this section is to study the effect of attractive forces on the phase diagram of smoothed collapsing spheres. For this, we generalize the potential by adding an attractive part to it:

$$\frac{U(r)}{\varepsilon} = \left(\frac{d}{r}\right)^n + \lambda_0 - \lambda_1 \tanh\left(k_1[r-\sigma_1]\right) + \lambda_2 \tanh\left(k_2[r-\sigma_2]\right), \qquad (12)$$

where $n = 14$, $k_1 = k_2 = 10$, and the values of parameters λ_i and σ_i are given in Table 1. We considered potentials with the steps $\sigma_1 = 1.15$ and 1.35. In Table 1, an ordinal number is assigned to each system. Below, we label the systems in accordance with the numbers in this Table. The potentials themselves are shown in Fig. 8.

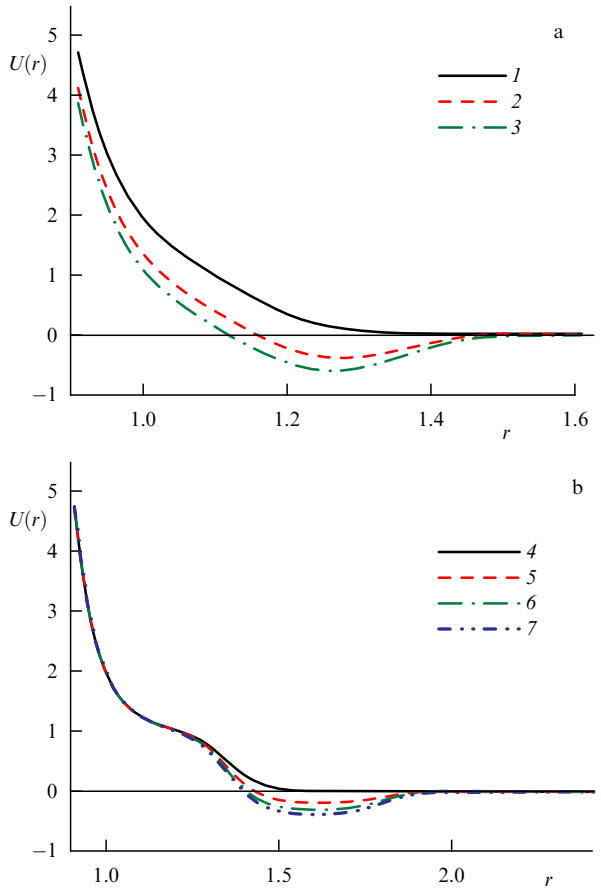

Figure 8. (Color online.) Potentials of generalized smoothed collapsing spheres (a) with the step $\sigma_1 = 1.15$ and different well depths w (*1*—$w = 0.0$, *2*—$w = 0.4$, *3*—$w = 0.6$; (b) with the step $\sigma_1 = 1.35$ and different well depths w (*4*—$w = 0.0$, *5*—$w = 0.2$, *6*—$w = 0.4$, *7*—$w = 0.6$).

Table 1. Parameters of the potential defined by Eqn (12). The last column gives the depth of the attractive well for parameters of the potential.

Number	σ_1	σ_2	λ_0	λ_1	λ_2	Well depth, w
1	1.15	0	0.5	0.5	0	0
2	1.15	1.35	0.2	0.5	0.30	0.4
3	1.15	1.35	0.07	0.5	0.43	0.6
4	1.35	0	0.5	0.5	0	0
5	1.35	1.80	0.5	0.6	0.10	0.2
6	1.35	1.80	0.5	0.7	0.20	0.4
7	1.35	1.80	0.5	0.8	0.30	0.6
8	1.35	1.80	0.5	0.9	0.40	0.8

3.1 Phase diagram of a system with the step $\sigma_1 = 1.15$ and attractive wells

We begin by studying the phase diagrams of systems with the step width $\sigma_1 = 1.15$. As we have seen in the preceding section, there is no reentrant melting in a purely repulsive system with this step. Its phase diagram is relatively simple, consisting of a liquid and a sequence of three crystal phases: fcc–bcc–fcc. In this section, we consider the effect of attraction on the phase diagrams of the system with the step $\sigma_1 = 1.15$.

The phase diagrams of systems with a purely attractive potential $w = 0$ and with the well $w = 0.4$ are compared in

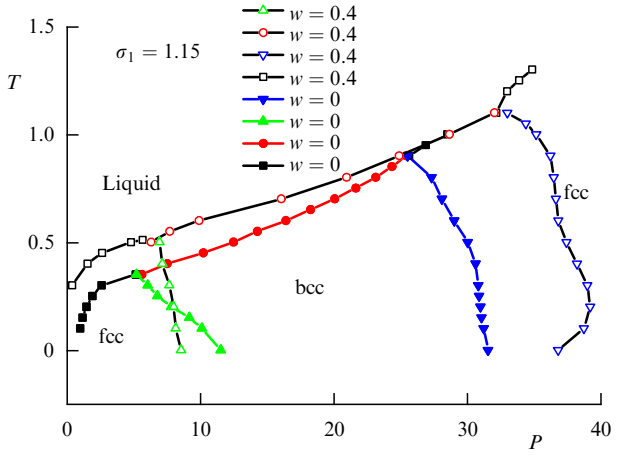

Figure 9. (Color online.) Comparison of the phase diagrams of systems of smoothed collapsing spheres with the step $\sigma_1 = 1.15$ and attractive wells $w = 0.0$ and $w = 0.4$ in $P-T$ coordinates.

Fig. 9. Qualitatively, the shape of the phase diagram remains the same as in the case of a purely repulsive potential. In precisely the same way the diagram shows the liquid phase domain and the fcc–bcc–fcc sequence. However, in comparison with a purely repulsive potential, the entire phase diagram is shifted upward and to the right: the stability domains of all crystal phases move to higher densities and higher temperatures.

On further deepening the attractive well, the crystal phases shift further to a higher temperature and density domains without any qualitative changes.

3.2 Phase diagram of a system with the step $\sigma_1 = 1.35$ and attractive wells

We turn to systems with the step width $\sigma_1 = 1.35$ and different well depths. We begin with a system with the well depth $w = 0.2$. The phase diagrams of this system are presented in Figs 10a and 10b. We can see that these phase diagrams resemble those of a purely repulsive system with the same step width. The crystal part of the phase diagram consists of low-density fcc, fct ($c/a = 1.6$), hexagonal, and high-density fcc phases. In comparison with a purely repulsive potential, the simple cubic phase is nonexistent in the system with the $w = 0.2$ well. Furthermore, the stability temperatures of low-density phases change: while the maximum of the melting temperature of the low-density fcc phase increased, the stability temperatures of the fct and hexagonal phases decreased. In addition, the 'gap' between the low-density fcc phase and the fct phase closed and the stability domain of the high-density fcc crystal shifted to lower densities.

Under a further increase in the attractive well depth ($w = 0.4$, $w = 0.6$, and $w = 0.8$), the general trend persists: the temperature of the maximum of the melting curve of the low-density fcc phase increases and the existence domain of the hexagonal phase decreases. In addition, the 'gap' reappears between the stability domains of different crystal structures.

We believe that in the region where no stable crystal phases have been detected, complex crystal structures may exist; however, they have not been detected in our work. As discussed above, the systems under consideration have the

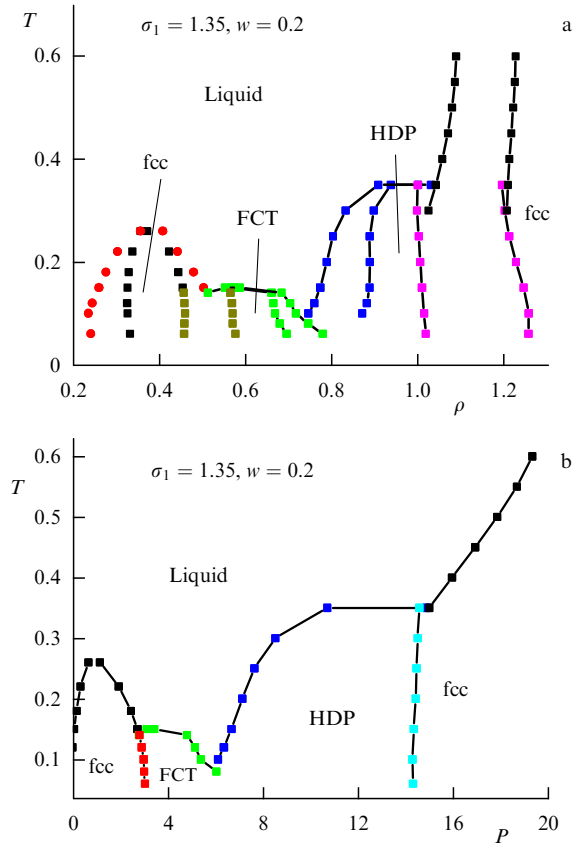

Figure 10. (Color online.) Phase diagram of a system of smoothed collapsing spheres with attraction with the step $\sigma_1 = 1.35$ and the well $w = 0.2$ in (a) $\rho-T$ and (b) $P-T$ coordinates.

property of quasibinarity, i.e. exhibit several properties characteristic of binary mixtures. The variety of structures that can be formed by two-component systems is quite large, which makes the quest difficult. Furthermore, the mixture structure is highly sensitive to the details of the interaction potential. Different parameterizations were proposed for binary LD mixtures in Refs [170] and [171]. After the names of their authors, these mixtures are respectively referred to as Kob–Andersen and Wahnström mixtures. The crystallization of the Kob–Andersen mixture was studied in Ref. [172]. The Kob–Andersen system was found to crystallize into the CsCl structure. The Wahnström mixture crystallization was investigated in Ref. [173]. This system was shown to crystallize into the $MgZn_2$ structure. These results suggest that owing to the quasibinarity, very complex structures can be observed in a system of smoothed collapsing spheres, both with and without attraction.

4. Anomalous behavior of a generalized system of smoothed collapsing spheres

As mentioned above, systems with a core-softened potential can exhibit anomalous behavior in the liquid phase, similar to the anomalous behavior of water. We next discuss three types of water-like anomalies [154–158, 184–190]: (1) the diffusion anomaly, in which the diffusion coefficient increases under isothermal liquid compression; (2) the density anomaly, whereby the thermal expansion coefficient of the liquid takes negative values corresponding to compression of the

liquid under isobaric heating. At the same time, when the liquid is heated along an isochore, the temperature dependence of the pressure has a minimum. In this paper, the position of the density anomaly is determined just from the minimum on the isochore of the system; (3) the structural anomaly, which manifests itself in the liquid becoming less structured under isothermal compression, i.e., its excess entropy increasing. Several different methods for determining the degree of the liquid structuredness were compared in Ref. [174], and it was shown that the method of choice relies on the excess entropy $S_{ex}(\rho, T) = S(\rho, T) - S_{id}(\rho, T)$, where $S_{id}(\rho, T)$ is the entropy of the ideal gas under the same density and temperature.

The emergence of anomalous behavior in such systems can be qualitatively explained as follows. As already discussed, the systems under study can be treated as quasibinary, which is due to the existence of two scale lengths in the system: the potential core σ and the repulsive step width σ_1. As shown above, the main role can be played by one of the scale lengths at different densities and temperatures. Specifically, at low densities and temperatures, particles are separated by a distance defined by the step size, while at high temperatures by a distance defined by the potential core σ. In the intermediate density domain, both characteristic scale lengths exert a strong influence on the properties of the system. It is this influence that gives rise to a sequence of several crystal structures. The interaction of different parameters of the system also affects the liquid properties. Specifically, at a low density near the low-density fcc phase, the coordination number of the liquid is close to 12, which corresponds to the proximity to the melting line of the fcc crystal. At the same time, the maximum of the first RDF peak is at $r = \sigma_1$, which means that although the liquid structure is rather densely packed, the packing itself can be compressed. As the density increases, the particles begin to 'fall through' and approach to a distance equal to the potential core width. As this takes place, the coordination number corresponding to the distance $r = \sigma_1$ begins to shorten, while the number of nearest neighbors at the distance σ, i.e., at the core, increases. Therefore, although the density increases, a larger volume becomes available for the motion of particles. The appearance of this additional volume can entail a significant change in all properties of the system. For instance, when larger space becomes available for particle motion, we can expect an increase in the diffusion coefficient, i.e., the appearance of a diffusion anomaly. On the other hand, the liquid structured at the distance σ_1 transforms into a liquid with a small number of particles at the distance σ and a defect structure at the distance σ_1. Therefore, with increasing density, the level of the liquid structuredness can decrease. Lastly, the advancement of some number of particles to the potential core distance and its related structure 'impairment' can facilitate the 'fall' of other particles to the distance σ, which would result in a density anomaly. Therefore, the physical reason for anomalous behavior in systems with two characteristic scale lengths can be the competition between the two local liquid structures determined by these scales lengths.

4.1 Anomalous behavior of a system with a purely repulsive potential

Figure 11 shows the diffusion coefficients along isotherms, the equations of state $P(T)$ along isochores, and the excess entropy along isotherms of a system with $\sigma_1 = 1.35$. We can see that all three anomalies are present in the system. We determine the existence domains of the anomalies in the $\rho - T$ plane. Figure 11a shows the density dependence of the system diffusion coefficient. The ascending parts of the curves, which end with maxima, correspond to the anomalous diffusion domains. The positions of diffusion coefficient maxima in the $\rho - T$ plane bound the existence domain of the diffusion anomaly. Similarly, the positions of excess entropy maxima in Fig. 11c define the existence domain of the structural anomaly. The behavior of the pressure as a function of the temperature along isochores is depicted in Fig. 11b. In a normal liquid, this is an ascending function. The boundary of the density anomaly is determined from the position of the minimum on this curve. This follows from the simple

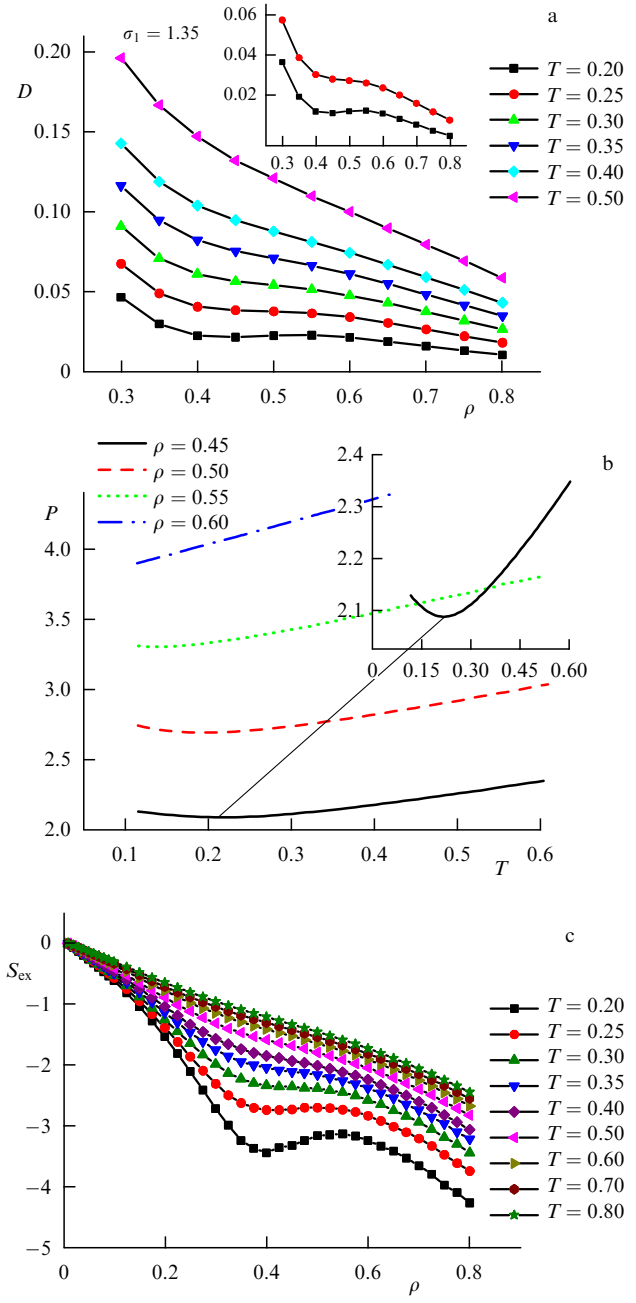

Figure 11. (Color online.) (a) Diffusion coefficient along a set of isotherms for a system with $\sigma_1 = 1.35$. (b) Equation of state $P(T)$ along a set of isochores for a system with $\sigma_1 = 1.35$. (c) Excess entropy S_{ex} along a set of isotherms for a system with $\sigma_1 = 1.35$.

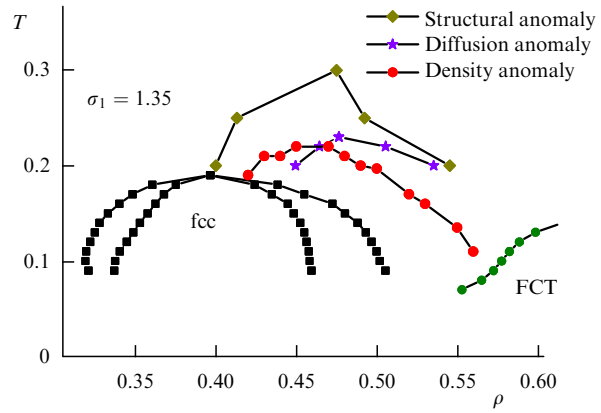

Figure 12. (Color online.) Domains of anomalous behavior of the system of smoothed collapsing spheres with $\sigma_1 = 1.35$.

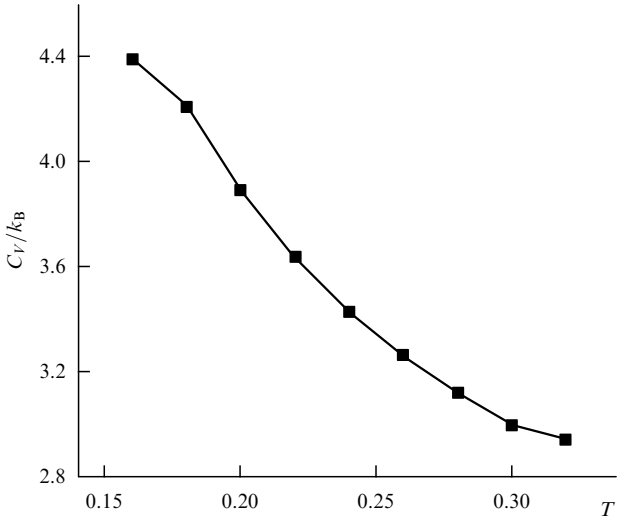

Figure 13. Heat capacity of the system of smoothed collapsing spheres with $\sigma_1 = 1.35$ in relation to the temperature for $\rho = 0.5$.

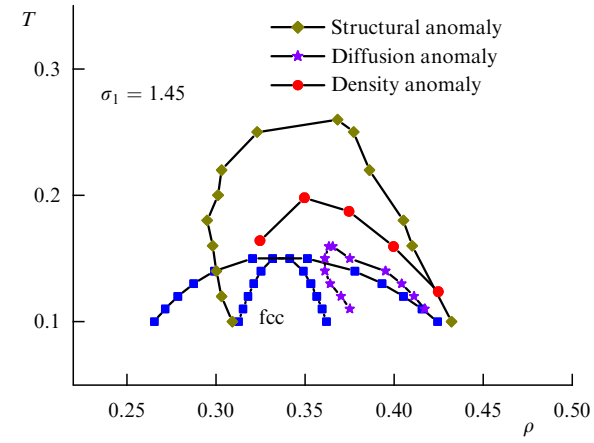

Figure 14. (Color online.) Domains of anomalous behavior of the system of smoothed collapsing spheres with $\sigma_1 = 1.45$.

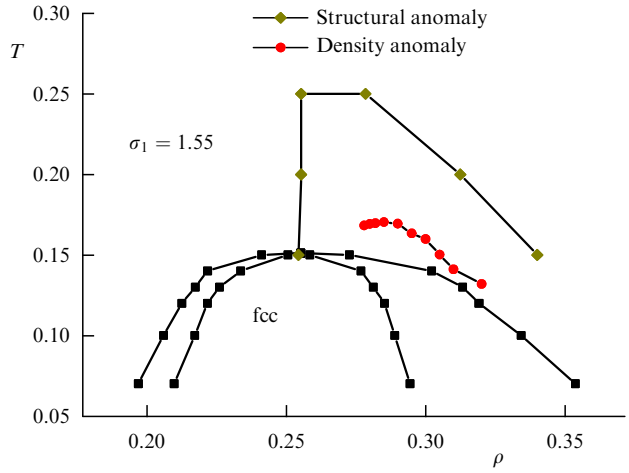

Figure 15. (Color online.) Domains of anomalous behavior of the system of smoothed collapsing spheres with $\sigma_1 = 1.55$.

thermodynamic relation $K_T(\partial P/\partial T)_V(\partial T/\partial\rho)_P = -N/\rho^2$, where K_T is the isothermal compressibility, which is always positive. We can see from Fig. 11b that $(\partial T/\partial\rho)_P > 0$ (which corresponds to $(\partial V/\partial T)_P < 0$) when $(\partial P/\partial T)_V < 0$, i.e., the density anomaly is observed at low temperatures. The resultant data are shown in Fig. 12. We note that Debenedetti et al. assumed that the domains of different anomalies in the $\rho - T$ plane are nested [91, 178]. Two nesting patterns could be identified: in water and in liquid silica. Observed in the case under consideration is a nearly water-like sequence of anomalies: the domain of the density anomaly is almost completely inside the diffusion anomaly domain, and both of them are encompassed by the structural anomaly domain. The anomalous behavior of other systems with a core-softened potential has been actively studied in the literature (see, e.g., Refs [179, 180] and the references therein). In this case, precisely the water-like arrangement of anomalies was revealed in all papers known to us. Figure 13 shows the temperature dependence of the heat capacity C_V in the anomalous domain for the system with $\sigma_1 = 1.35$. It is noteworthy that the heat capacity of this system is $4.4R$ in the neighborhood of the melting line [181, 182], unlike that of a normal liquid, which is close to $3R$ in this domain.

As the step width σ_1 increases, the anomalous behavior changes. Figure 14 shows the anomalous behavior domains for the system with $\sigma_1 = 1.45$. We can see that the mutual arrangement of the anomalies is different in this case: the diffusion anomaly moved to the lower part of the phase diagram and approached the melting curve of the low-density fcc phase. Next comes the density anomaly, which in turn is inside the structural anomaly domain. This anomaly order corresponds to neither water nor liquid silica and was first observed in our studies [184, 185]. It is pertinent to note that this anomaly arrangement had not been observed previously in experiment.

Figure 15 shows the arrangement of anomalous domains for the system with $\sigma_1 = 1.55$. We can see that the diffusion anomaly disappeared, while the density anomaly and the structural anomaly persist.

Lastly, observed in the system with $\sigma_1 = 1.8$ is only the structural anomaly (see Fig. 16).

We generalize the data for the systems with different step widths to obtain the following picture. Observed in the system with $\sigma_1 = 1.35$ is the water-like ordering of the anomalies: the density anomaly domain is inside the domain of anomalous diffusion, which in turn is encompassed by the structural anomaly domain. However, even in the system with

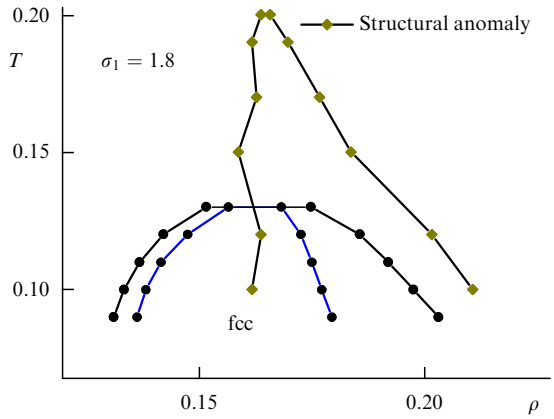

Figure 16. (Color online.) Domains of anomalous behavior of the system of smoothed collapsing spheres with $\sigma_1 = 1.8$.

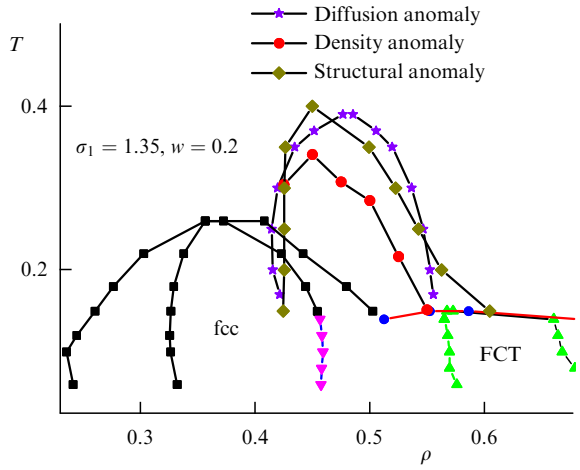

Figure 17. (Color online.) Domains of anomalous behavior of the system with $\sigma_1 = 1.35$ and $w = 0.2$ in the phase diagram in density–temperature coordinates $\rho - T$.

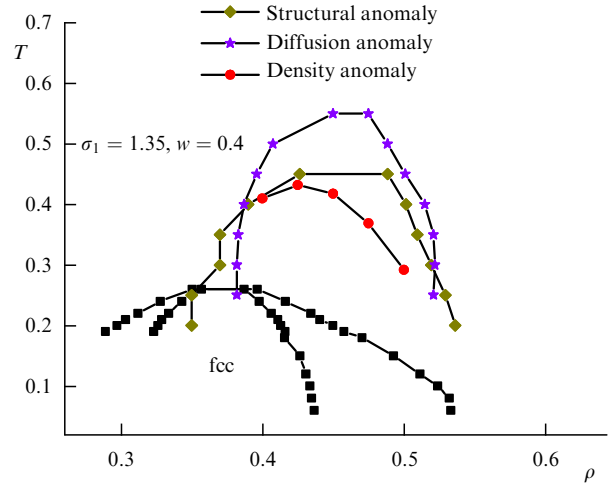

Figure 18. (Color online.) Domains of anomalous behavior of the system with a collapsing sphere potential with attraction (formula (12)), $\sigma_1 = 1.35$ and $w = 0.4$, in the phase diagram in density–temperature coordinates $\rho - T$.

$\sigma_1 = 1.45$, the situation is different: the anomalous diffusion domain is inside the density anomaly domain. In the system with $\sigma_1 = 1.55$, the diffusion anomaly vanishes, and in the system with $\sigma_1 = 1.8$, the density anomaly vanishes as well. The structural anomaly persists in all systems under consideration.

4.2 Effect of attraction on the anomalous behavior of smoothed collapsing spheres

We now consider the effect of the attractive part of the potential on the anomalous behavior of a liquid. As an example, we consider systems with $\sigma_1 = 1.35$ and with wells $w = 0.2$ and $w = 0.4$ [157, 184–190]. Figure 17 shows the arrangement of anomalous domains for the system with the well $w = 0.2$ and Fig. 18 shows the arrangement for the system with $w = 0.4$. As is clear from these figures, all curves shift towards higher temperatures with as the well depth increases. In this case, the rates of displacement of different curves turn out to be different again. As with step broadening, the diffusion anomaly domain turns out to be the 'fastest' one. For $w = 0.2$, it is almost equal to the structural anomaly and overgrows it for $w = 0.4$, such that the arrangement of anomalies becomes the same as in liquid silica [91, 189].

Therefore, in the framework of one model, we obtain three different arrangement orders for anomalous domains by varying the parameters of the potential: as in water, as in silica, and a third version, with the diffusion anomaly being inside the density anomaly. This suggests that the case of silica is not exceptional, as was hypothesized previously, and is defined by the features of interaction in this substance.

We recall that in Refs [91, 178] it was assumed that the anomalous domains, when depicted on the $\rho - T$ plane, are nested. Two nesting patterns were proposed: as for water (the anomalous density domain is inside the anomalous diffusion domain, which in turn is encompassed by the structural anomaly) and as for liquid silica (density–structure–diffusion, i.e., compared to water, inversion of the diffusion and structural anomalies occurred). As shown on a rigorous thermodynamic basis in Refs [179, 189], the density anomaly is always inside the domain of the structural anomaly. At the same time, the domain of anomalous diffusion behavior can be located anywhere. A similar behavior was discovered in our studies [184, 189] in the example of a model of smoothed collapsing spheres with attraction. Figure 19 schematically shows the mutual arrangement of anomalous domains determined in our work, including the water-like arrangement and an arrangement similar to the one observed in liquid silica. After that, the arrangement of anomalous domains was studied in many liquids. However, in all papers known to us, the resultant anomaly order was the same as for water. That is why the case of liquid silica seemed to be an unusual exception to the general rule. Our research radically changes the way we look at the situation: as is clear from the results described above, different nesting patterns can occur under variation of the potential parameters even in the framework of one model. This suggests the conclusion that liquid silica is not an exception but is characterized by some specific ratio of the particle interaction parameters responsible for this behavior [189].

Lastly, we briefly discuss two other significant aspects of the anomalous behavior of systems with negative-curvature potentials in the repulsion region (core-softened potentials). As mentioned in the Introduction in discussing the Widom line, an objection to this concept is the fact that the position of this line depends on the thermodynamic path along which the susceptibility maxima are calculated in the neighborhood of a critical point. A similar situation also occurs in the case of the

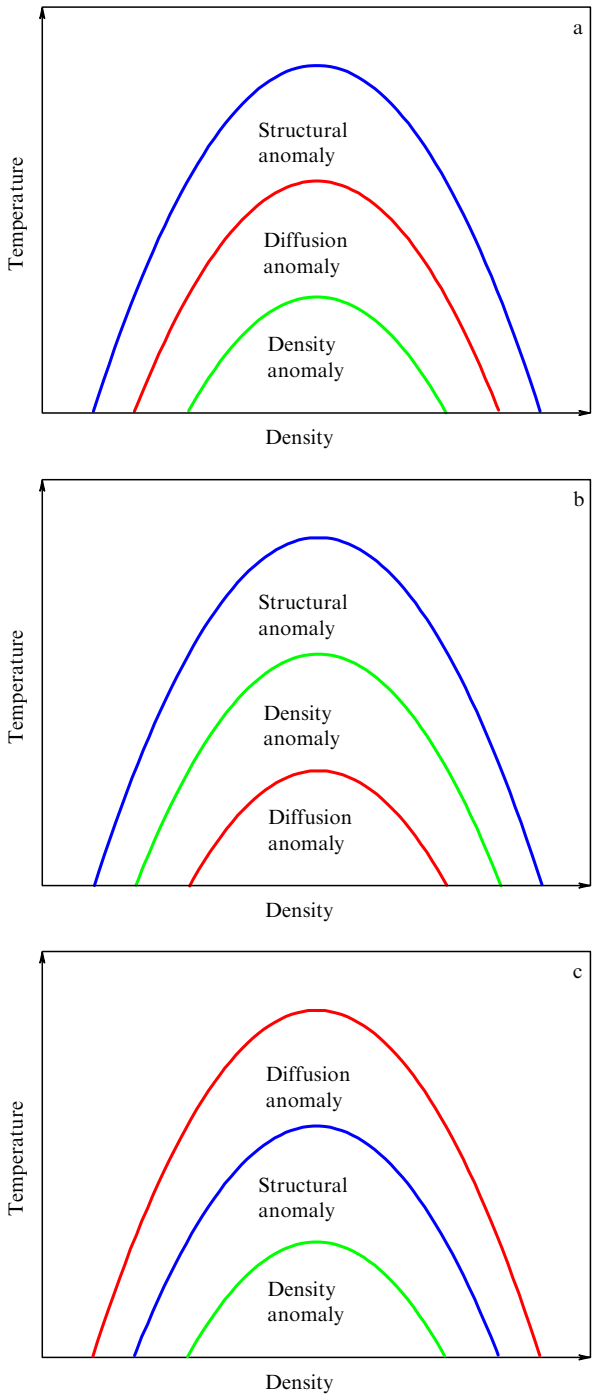

Figure 19. (Color online.) Arrangement of anomalous domains [184, 189] on the temperature–density plane $\rho - T$. The domain of anomalous density behavior is always inside the structural anomaly domain, while the diffusion anomaly can reside (a) between the structural anomaly and the density anomaly (see Fig. 12) (water-like behavior); (b) inside the density anomaly domain (not discovered experimentally); (c) outside of the structural anomaly domain (behavior similar to liquid silica, Fig. 18).

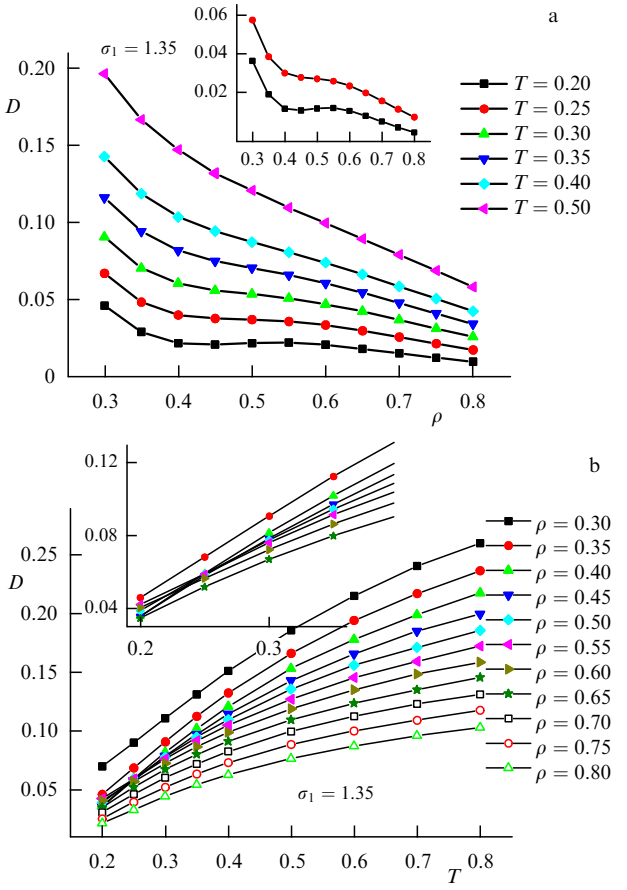

Figure 20. (Color online.) Diffusion coefficient of the system with potential (11) ($\sigma_1 = 1.35$) along (a) isotherms and (b) isochores. The inset in Fig. 20a shows low-density isotherms [186–188].

anomalous behavior of the systems under consideration. As shown in Refs [186–188], the anomalous behavior depends on the trajectory in the space of thermodynamic variables $T-\rho-P$ along which the calculation (or measurement) of a specific thermodynamic or dynamic quantity is performed. For example, Fig. 20 shows the behavior of the diffusion coefficient as a function of density along isotherms and as a function of temperature along isochores. As can be seen from Fig. 20a, for relatively low temperatures, it is sufficient to calculate (or measure) one isotherm to draw a conclusion regarding the anomalous system behavior. At the same time, there is no way of reaching the conclusion of anomalous behavior from a single isochore: required is a set of isochores, whose intersection is an indication of the diffusion anomaly. A similar situation takes place for the other anomalies, the density and structure ones.

As discussed in the Introduction, a possible explanation of the anomalous behavior of water is the existence of the critical liquid–liquid transition point [96–98], which is located deep in the metastable supercooled domain, supposedly unattainable in normal experiments. The existence of Widom's line corresponding to this critical point was hypothesized in Ref. [49]. In computer simulations, attempts have been made to find the liquid–liquid transition in systems with a core-softened potential [88, 124–127, 135, 136], but in this case the Widom line had a positive slope in the $P-T$ coordinates, which does not coincide with the slope of a real transition [49]. In this connection, it is pertinent to note that the authors of Ref. [189] discovered an analogue of the Widom line for potential (11). This potential is purely repulsive, and therefore attempts to discover the liquid–liquid phase transition in this system have not met with success. However, in the anomalous region, it was possible to discover maxima of the heat capacity C_P and compressibility K_T, as well as a minimum of the thermal expansion coefficient α_P. This permitted hypothesizing the existence of a

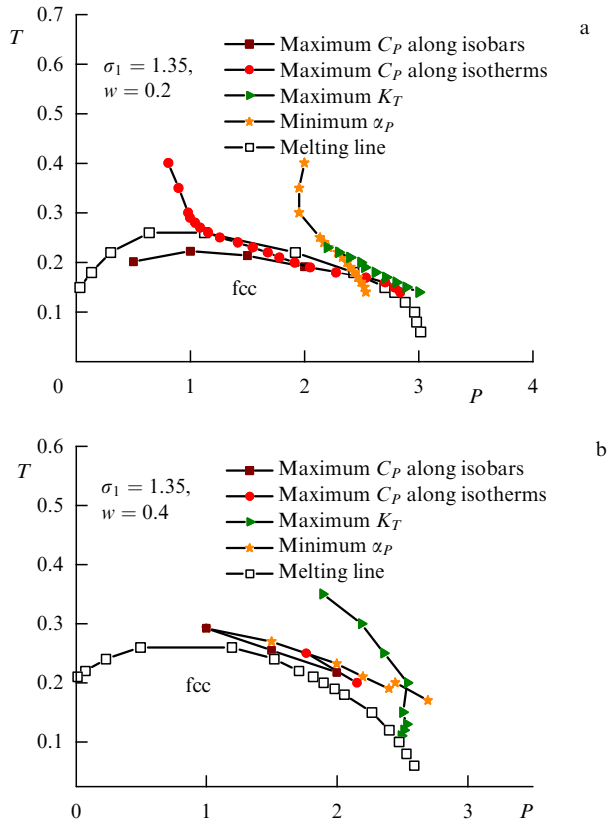

Figure 21. (Color online.) Lines of maxima for the isobaric heat capacity C_P along isobars and isotherms, lines of maxima for the compressibility K_T along isotherms, and lines of minima for the thermal expansion coefficient α_P along with the melting line for systems with potential (12) with (a) $w = 0.2$ and (b) $w = 0.4$ [189].

virtual critical point located in the negative temperature domain. In this case, the slope of the analogue of Widom's line corresponds to the slope of Widom's line for the liquid–liquid transition in water [49] (see Fig. 21). We note that the critical point of the liquid–liquid transition was found in Refs [159, 160] for a somewhat different set of parameters of potential (12).

5. Phase diagrams and anomalous behavior of two-dimensional systems

In this section, we consider how the space dimensionality affects the melting scenario and the anomalous behavior of the systems considered in the previous sections. It is well known that the crystal state is nonexistent in the one-dimensional case, and therefore we address the case of two-dimensional systems, which is by far more interesting and complex. The melting of two-dimensional systems was considered at length in recent review [191] (see also Refs [192–194]). Unlike three-dimensional systems, which always melt via a single first-order transition on the strength of symmetry considerations, fully developed fluctuations in two dimensions result in a radical change in the possible scenarios of melting.

As is commonly known, the crystal phase differs from an isotropic liquid by the existence of two broken symmetries: translational and orientational. Peierls, Landau [195–197], and, based on the Bogoliubov theorem [198–200], more recently Wagner and Mermin [201–203] showed that the long-range crystal (translational) order cannot exist in two dimensions owing to thermodynamic fluctuations and transforms into a quasi-long-range order characterized by a slow power-law decay of order-parameter correlations. On the other hand, the true long-range orientational order (the order in the orientations of 'bonds' connecting a molecule to its nearest neighbors) does take place in two dimensions, as first noted by Mermin [203] (see also Ref. [191]). An ordinary isotropic liquid exists at high temperatures.

As shown by Berezinskii, Kosterlitz, and Thouless (BKT) [204–206] (see also Refs [191, 193, 194]), the quasi-long-range order in degenerate two-dimensional systems, to which two-dimensional crystals also belong, breaks down due to the dissociation of coupled topological defects. In the case of the XY model, for instance, these are vortices. Even in the original work [207], Kosterlitz and Thouless noted that a two-dimensional crystal should melt via the dissociation of dislocation pairs, which are topological defects in this case. These defects are well defined in the presence of quasi-long-range translational order. In a two-dimensional crystal, apart from quasi-long-range translational order, there is long-range orientational order, and therefore, as noted later by Halperin and Nelson [208, 209] (see also Ref. [210]), the liquid turns out to be anisotropic above the point of dislocation-pair dissociation. They found that the dissociation of dislocation pairs does not break the long-range orientation order completely but merely transforms it into a quasi-long-range one [191]. The resultant new phase received the name 'hexatic' by analogy with liquid crystals, but, unlike liquid crystals, it is realized in systems with isotropic potentials. In the framework of a rather crude analogy, the hexatic phase can be thought of as an ordered system of hexagonal clusters consisting of a molecule and its six nearest neighbors. In this case, the correlation function of the orientational order parameter for a system of hexagons decays with distance in accordance with a power law (quasi-long-range orientational order). In the hexatic phase, free dislocations exist, and its shear modulus is therefore equal to zero, i.e., it is a liquid with elements of ordering. We note that a dislocation can be represented as a coupled pair of two disclinations. The hexatic phase transforms into an ordinary isotropic liquid as a result of the subsequent BKT transition via dissociation of disclination pairs. The presented theory bears the name Berezinskii–Kosterlitz–Thouless–Halperin–Nelson–Young (BKTHNY) theory. In the framework of this theory, a two-dimensional crystal should melt via two continuous BKT transitions with an intermediate hexatic phase.

The BKTHNY theory was very popular for a long time and gave rise to a wealth of publications, both theoretical papers reliant on computer simulations and experimental ones (see the references in Ref. [191]). Based on both experiments (see, e.g., Refs [211–215]) and computer simulations [216], today it is valid to say that systems with a long-range interaction (for instance, Coulomb or dipole–dipole interactions, and soft spheres $1/r^n$ with exponents $n \leqslant 6$) melt according to the BKTHNY scenario.

At the same time, the standard first-order transition can also be realized. The possible mechanisms of this transition were proposed, e.g., in Refs [191, 217–222]. It turns out in this case that the leading role in determining the transition type is played by the energy of the topological defect (dislocation) core: for a low core energy, two-dimensional melting can occur as a first-order transition as a result of, say, the formation of grain boundaries [217, 218] or the dissociation

of disclination quadrupoles. In the crystallization theory, it was shown using the density functional method that the melting scenario depends on the shape of the intermolecular potential [223–230], but a detailed description of two-dimensional melting scenarios in relation to the form of the potential requires the use of computer simulations in the majority of cases [191].

However, proposed recently was one more scenario [216, 232–234], whereby the crystal-to-hexatic phase transition is a continuous BKT transition, while the hexatic phase transforms into an isotropic liquid via a first-order transition. This scenario is supposedly true for soft-sphere systems $1/r^n$ with $n > 6$ [216, 235], including the two-dimensional systems of hard spheres [236]. As discussed in Ref. [191], today there is no consistent theory of a first-order transition from the hexatic phase to an isotropic liquid. The possible mechanism is that the BKT transition can become a first-order transition as the core energy of the topological defect decreases [237–244].

It is noteworthy that presently there are no clear theoretical criteria that make it possible to unambiguously determine, proceeding from the type of the potential, which melting scenario would be realized. We recall that the BKTHNY theory, like computer simulations of soft spheres [216, 235] and experiments on two-dimensional hard spheres [236], pertains to a triangular crystal lattice. However, two-dimensional systems with square and more complex lattices (see, e.g., Refs [245, 246]) were found recently to which the existing theories can be applied only conventionally to investigate the melting scenarios. Furthermore, as discussed in Refs [235, 247], random pinning is capable of changing the melting scenario and transforming a first-order transition into two-stage melting involving a continuous crystal-to-hexatic phase transition and a first-order transition from the hexatic phase to the isotropic liquid. Therefore, studying the relation between the shape of the interparticle potential and the existence of the hexatic phase is an interesting problem, which has yet to be unambiguously solved.

5.1 Two-dimensional system with the potential of smoothed collapsing spheres

We consider two systems that exhibit nontrivial melting scenarios in two dimensions [248–252]. The first is the system of smoothed collapsing spheres with potential (11). The melting of systems with 20,000 to 100,000 particles was simulated by the method of molecular dynamics (LAMMPS package) [254] in NVT and NVE ensembles. Several methods were used to determine the phase transition boundaries. Primary estimates relied on an analysis of the equations of state. In the case of first-order transitions, Mayer–Wood loops [255] (a two-dimensional analogue of Van der Waals loops) should be observable in the equations of state, which are practically absent for continuous transitions for this number of particles. The equations of state quite reliably reflect the transition domains, i.e., the coexistence domains of two phases, but do not provide information about the transition scenario. To exactly determine the stability boundaries of the hexatic phase and the crystal in these simulations, we used an approach involving the long-range behavior of the orientational and translational correlation functions of the order parameters, which was first proposed in our study [247]. As first shown in Ref. [209], the hexatic phase stability boundary can be determined from the behavior of the orientational correlation function (OCF) $G_6(r) \propto r^{-\eta_6}$, whose exponent must be $\eta_6 = 1/4$ in the hexatic-to-isotropic

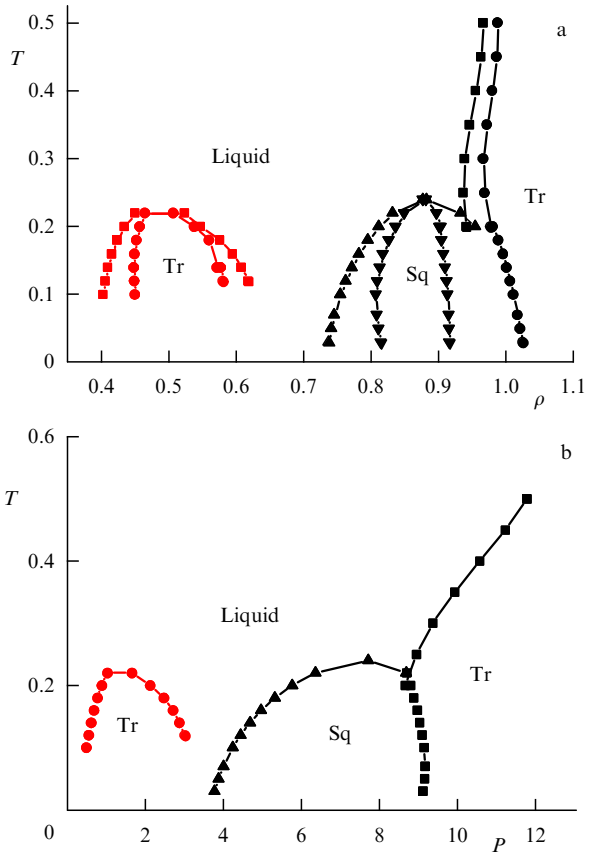

Figure 22. (Color online.) Phase diagram of the two-dimensional system with potential (11) and $\sigma_1 = 1.35$ in (a) $T-\rho$ and (b) $T-P$ coordinates. Tr — triangular lattice, Sq — square lattice.

liquid transition, while the translational correlation function (TCF) also exhibits a power-law decay $G_T(r) \propto r^{-\eta_T}$ with the exponent $\eta_T = 1/3$ in the crystal–hexatic transition.

The presence of orientational and translational ordering in the system was estimated by studying the behavior of the corresponding order parameters and their correlation functions.

A series of papers [248–250] (see also Refs [191, 256]) was concerned with the study of the behavior of two-dimensional systems with potential (11) and $\sigma_1 = 1.35$. These papers were discussed at length in our previous review [191], and we therefore briefly recall the main results and their further development [251].

Figure 22 shows the phase diagram calculated by the method of tangents to the Helmholtz free energy curves for crystal and liquid phases [161]. This phase diagram is to be compared to the three-dimensional case (see Fig. 7). The phase diagram in Fig. 22 corresponds to the assumption that all transitions are of the first order. As discussed in Ref. [191], this phase diagram is the domain of absolute crystal stability. However, the instability to dislocation pair dissociation can emerge at a lower temperature T_m, which results in melting via a continuous BKT transition. Applying criteria based on the behavior of the correlation functions of orientational and translational order parameters permits elaborating the melting scenario. As it turns out (see Fig. 12 in Ref. [191]), at high densities, the system melts via a first-order transition. The transition between different crystal structures is also a first-order transition. At low densities, the situation is more

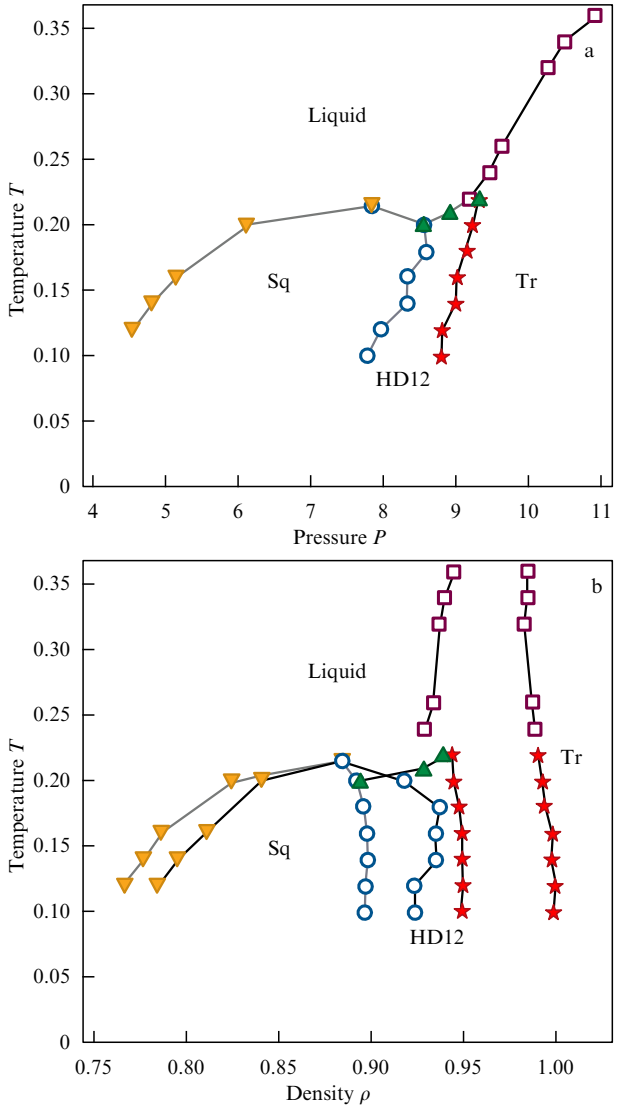

Figure 23. (Color online.) Elaborated phase diagram of the two-dimensional system with potential (11) with $\sigma_1 = 1.35$ at high density (see Fig. 22) in (a) $T-P$ and (b) $T-\rho$ coordinates (Tr — triangular lattice, Sq — square lattice, HD12 — dodecagonal quasicrystal) (see Ref. [251]).

complicated: the melting in the left branch of the phase diagram occurs via a first-order transition, and in the right branch via a continuous crystal–hexatic transition and a hexatic–isotropic-liquid first-order transition [191]. In this case, random pinning may qualitatively change the melting scenario in the case of a first-order transition and convert this transition into two: a continuous crystal–hexatic BKT transition and a first-order hexatic–isotropic-liquid transition [235, 247].

The shape of the two-phase domain for the square-to-triangular lattice transition (Fig. 22a) suggests that another, more complex, domain may reside between these two crystal phases. Recently, in [251], a dodecagonal quasicrystalline structure was indeed discovered in this domain (see Fig. 23).

As in the case of three dimensions, the system with potential (11) exhibits anomalous behavior in the two-dimensional case. However, as is evident in Fig. 24, observed in this case is the inversion of the structural anomaly and the diffusion anomaly, the ordering of the anomalies becoming the same as in liquid silica (see Fig. 18).

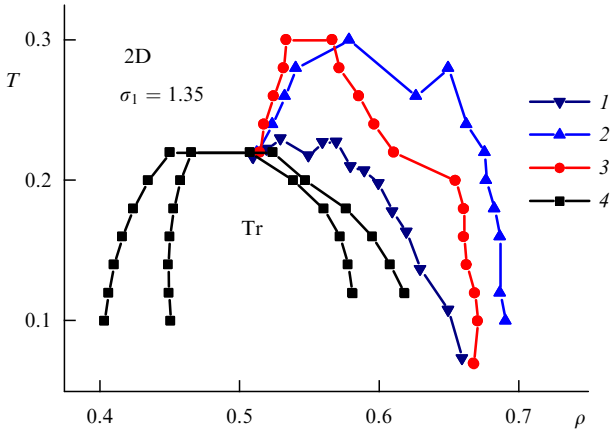

Figure 24. (Color online.) Boundaries of anomaly domains in 2D: *1* — density anomaly; *2* — diffusion anomaly D; *3* — structural anomaly; *4* — boundary of triangular crystal Tr at a low density. The ordering of the anomalies is the same as in liquid silica (see Fig. 18): the density anomaly domain is inside the structural anomaly domain, which in turn is inside the diffusion anomaly domain.

5.2 Two-dimensional system with the Hertzian potential

An even more interesting behavior of two-dimensional melting scenarios is exhibited by a system with the Hertzian potential [252], which is of the form

$$U(r) = \begin{cases} \varepsilon\left(1 - \dfrac{r}{\sigma}\right)^{5/2}, & r \leqslant \sigma\ , \\ 0\,, & r > \sigma\,. \end{cases} \qquad (13)$$

This potential corresponds to the deformation energy of elastic balls under uniaxial compression [257]. The parameter ε is related to the elastic ball characteristic as

$$\varepsilon = \frac{2}{15}\,\frac{E\sigma^3}{1-\nu^2}\,,$$

where E is Young's modulus and ν is the Poisson coefficient of the ball material. Strictly speaking, potential (13) applies only to small deformations and cannot be used at strong compressions and densities. However, it turns out that it can be used to qualitatively describe the behavior of soft uncharged macromolecules such as polymer globules and star-shaped polymers.

The phase diagram of a three-dimensional system with the Hertzian potential was analyzed by computer simulation techniques in the well-known work by Frenkel et al. [258], who showed that the phase diagram consists of a large number of crystal phases. Furthermore, they discovered anomalous diffusion behavior in this system. More recently, a structural anomaly was discovered in this system [158].

The authors of Refs [259–261] reported a number of interesting results concerning the behavior of the two-dimensional Hertzian system, including the preliminary form of the phase diagram, the discovery of a quasicrystalline phase, and low-density melting scenarios.

In our work [252], the phase diagram of Hertzian spheres was studied in two stages. At the first stage, a system comprising 4000 particles was simulated by the method of molecular dynamics. The system was modeled in a rectangular box with periodic boundary conditions. We considered the density interval from $\rho_{\min} = 0.6$ to $\rho_{\max} = 10.0$ with the

density increment $\Delta\rho = 0.2$. The system simulation included 5×10^7 steps with the time increments $dt = 0.001$. Approximate phase boundaries were determined at the second stage. For this, we studied the equations of state of the system, the radial distribution functions, and diffraction patterns.

Figure 25 shows the resultant phase diagram. We note that density steps in two-dimensional systems are typically quite small, and hence the width of the two-phase domain turns out to be smaller than the size of symbols. We can see that the phase diagram is extremely complicated. It is characterized by the existence of a large number of different phases, including complex structures like a dodecagonal quasicrystal.

At the second stage, we studied the existence domains of triangular and square crystals of low density in more detail for the purpose of determining the melting scenarios of these systems. A system of 20,000 particles was modeled for the triangular crystal and a system of 22,500 particles for the square one. We studied the equation of state, the orientational and translational order parameters, and their correlation functions.

We first consider the melting of the left branch of a triangular crystal (see Fig. 25). Figure 26a shows an isotherm of the system in the transition from a crystal to a liquid. This isotherm is marked with the points of the loss of stability of the crystal and hexatic phases, obtained from the conditions $\eta_T = 1/3$ for the exponent of the translational correlation function and $\eta_6 = 1/4$ for the exponent of the orientational correlation function, which are shown in Figs 26b and 26c. The resultant data allow a conclusion that the crystal-to-hexatic transition is continuous, while the hexatic-to-liquid transition is a first-order one.

A different picture is observed for the melting of the right branch of a low-density triangular crystal (Figs 27a–c). As can be seen from the figures, the right branch of the triangular crystal melts in accordance with the BKTHNY scenario.

We consider the melting of a square crystal similarly. Figure 28 shows the equations of state in crossing the square-crystal melting line in the directions of decreasing and increasing density. We can see that the equations of state exhibit loops in both cases, which testify to the existence of a first-order transition in the system. However, in the consideration of the system correlation functions (Figs 29a–d), it turns

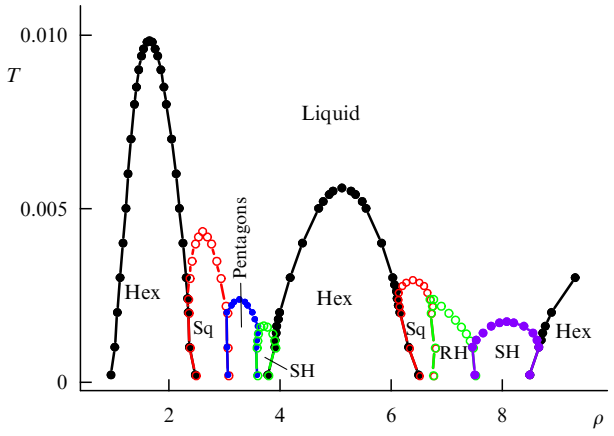

Figure 25. (Color online.) Phase diagram of a two-dimensional system of Hertzian spheres. Hex — triangular phase, Sq — square phase, Pentagons — dodecagonal quasi-crystal, SH — triangular phase extended in one direction, RH — rhombohedral phase.

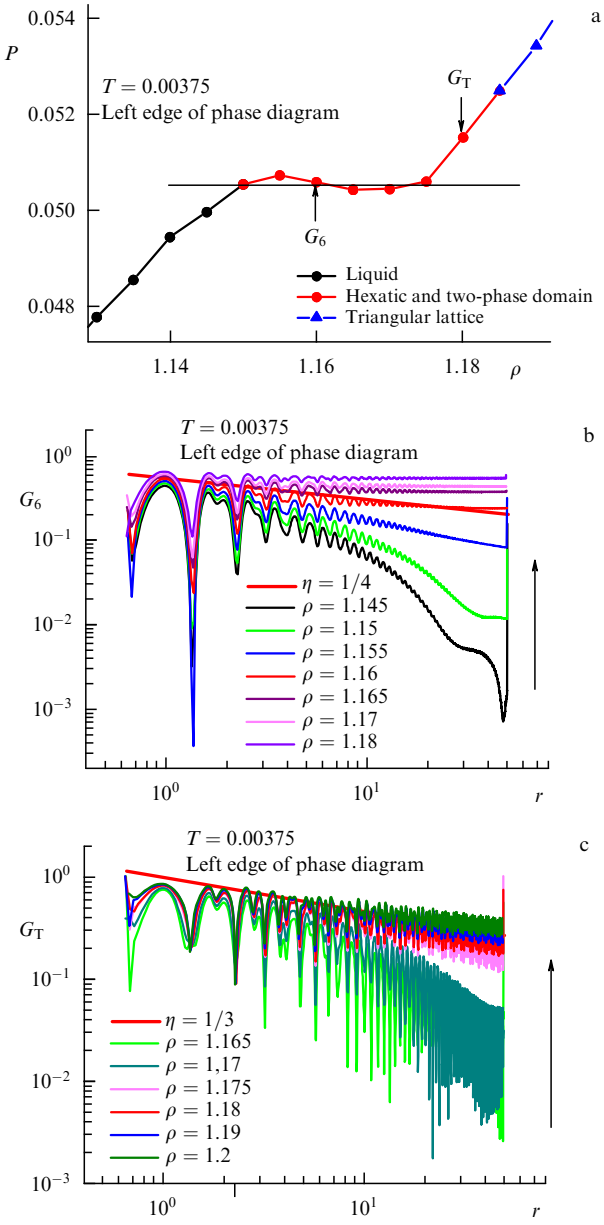

Figure 26. (Color online.) (a) Equation of state of the system of Hertzian spheres for $T = 0.00375$ in crossing the melting line in the direction of decreasing density. (b) Correlation function of the orientational order parameter along the same isotherm. (c) Correlation function of the translational order parameter along the same isotherm.

out that the left and right branches melt according to different scenarios. The crystal and tetratic stability limits are plotted on the equations of state in Fig. 28. We can see that the left branch of the phase diagram melts according to a third scenario (a crystal-to-tetratic BKT transition and a tetratic-to-isotropic-liquid first-order transition), while the right one melts according to a crystal-to-liquid first-order transition.

The resultant data permit constructing a phase diagram of Hertzian spheres at low densities (see Fig. 30). We can see that the diagram is extremely complicated. Apart from the usual crystal and liquid phases, existence domains of hexatic and tetratic phases appear.

We take a closer look at the neighborhood of the liquid–hexatic–tetratic triple point. Figure 31 shows the system equations of state in its neighborhood. We can see from

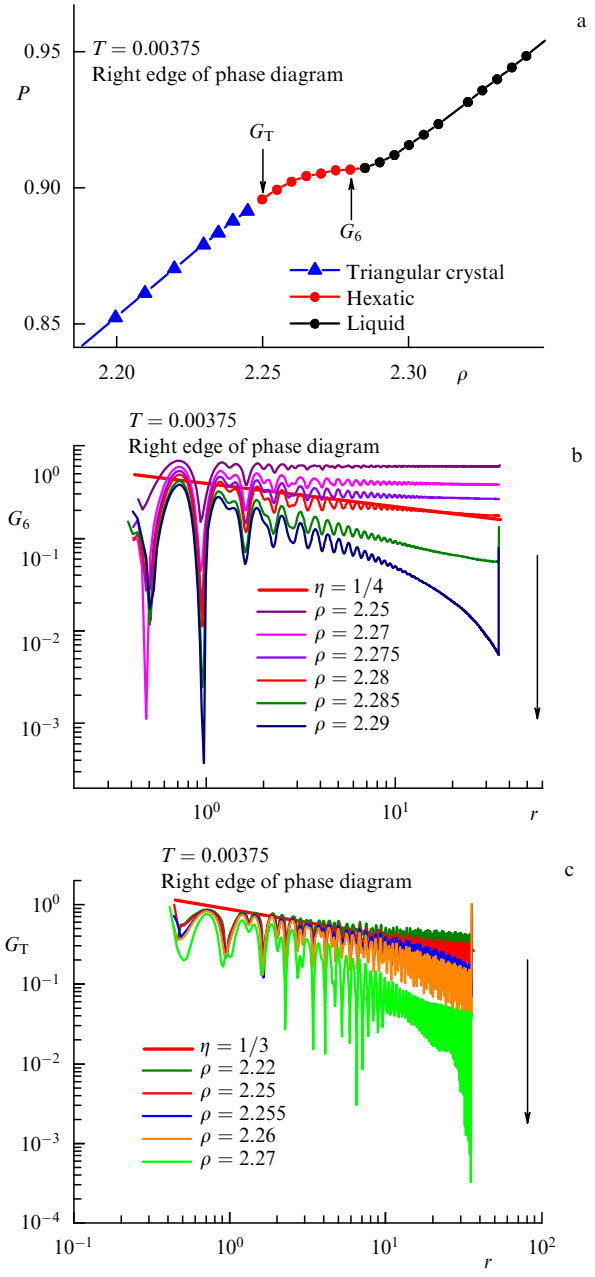

Figure 27. (Color online.) (a) Equation of state of the system of Hertzian spheres for $T = 0.00375$ in crossing the melting line in the direction of increasing density. (b) Correlation function of the orientational order parameter along the same isotherm. (c) Correlation function of the translational order parameter along the same isotherm.

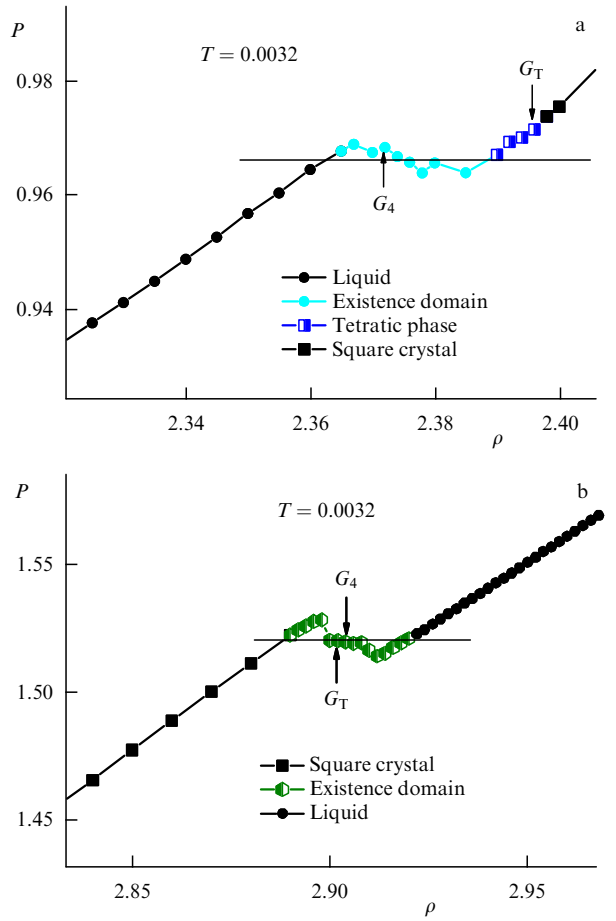

Figure 28. (Color online.) (a) Equation of state of the system of Hertzian spheres for $T = 0.00375$ in crossing the square-crystal melting line in the direction of decreasing density. (b) The same in the direction of increasing density.

these equations of state that the system exhibits two special features. First, a loop appears in the equations of state as the temperature decreases. We saw above that the right branch of the triangular phase melts via the BKTHNY scenario. The resultant equations of state allow a conclusion that as the temperature decreases, the system passes through a tricritical point and returns to the third melting scenario.

The second feature of the resultant equations of state is the decrease in pressure as the temperature increases. This is an indication of a density anomaly in the system. Figure 32 depicts the system isochores. We can see that a minimum appears on these isochores, which confirms the existence of a density anomaly. The position of the anomalous density domain is shown in Fig. 30.

Therefore, in two dimensions in the framework of one relatively simple phenomenological potential, it is possible to obtain a broad range of physical properties: a complicated phase diagram with a large set of crystalline structures, including quasicrystalline states, anomalous behavior in the liquid phase, and the amazing fact that the system can melt in accordance with different melting scenarios in different parts of the phase diagram, which is absolutely impossible in the three-dimensional case.

6. Conclusions

Studies of so-called soft matter, which includes protein solutions, polymers, colloids, and dust plasma, have to a certain extent rekindled interest in the statistical mechanics of systems described by relatively simple isotropic effective potentials, which are well suited for analysis by computer simulation techniques. Considering the relatively large size of colloidal particles (from ≈ 10 nm to ≈ 10 μm), it is clear that an ab initio calculation of interparticle interactions is presently an insoluble problem. That is why the properties of these systems can mostly be predicted with the use of effective potentials, which define the structure of soft matter, its collective dynamics, and its thermodynamics. A distinctive feature of soft matter is the possibility of varying the shape of the potentials at a microscopic level (adjustable potentials),

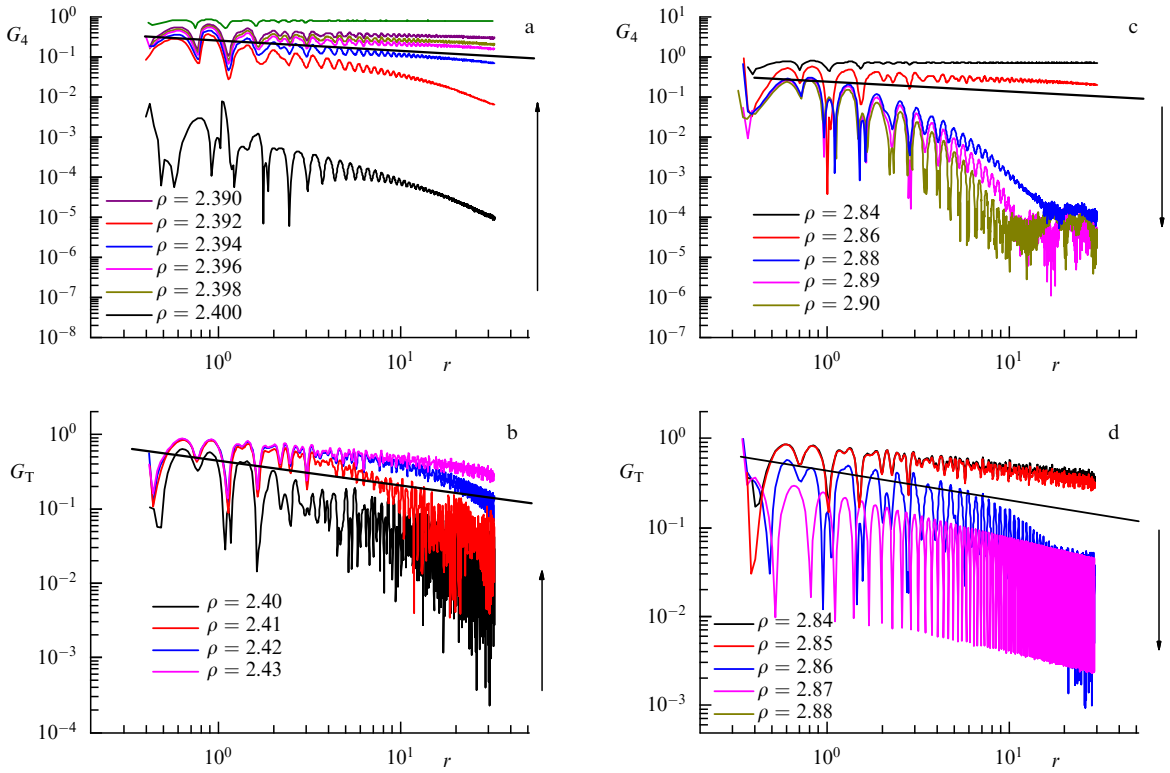

Figure 29. (Color online.) (a) Orientational correlation function for $T = 0.0032$ in the transition from a square crystal in the direction of decreasing density. (b) Translational correlation function in the transition in the direction of decreasing density. (c) Orientational correlation function in the transition from a square crystal in the direction of increasing density. (d) Translational correlation function in the transition in the direction of increasing density.

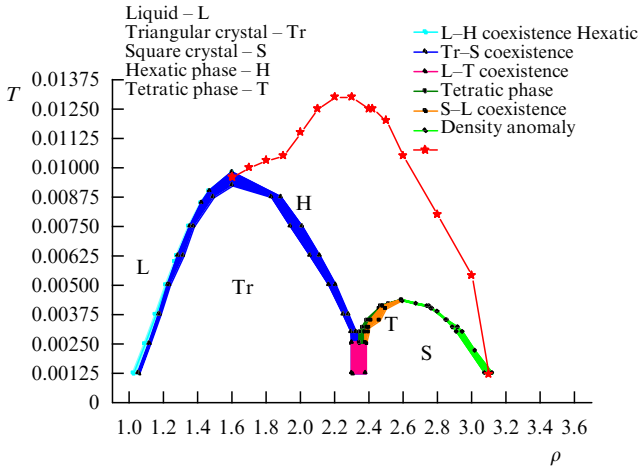

Figure 30. (Color online.) Phase diagram of a system of Hertzian spheres at low temperatures.

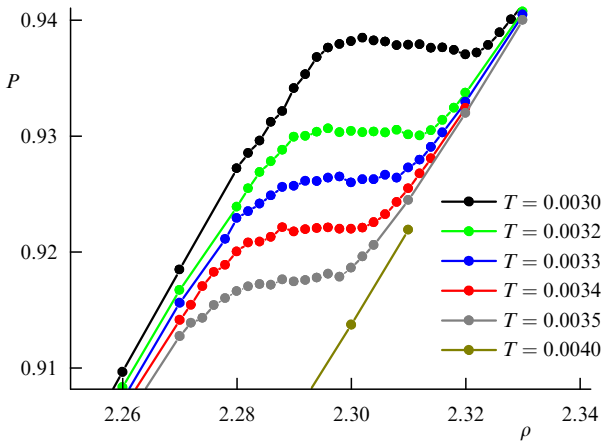

Figure 31. (Color online.) Equations of state of a system of Hertzian spheres in a neighborhood of the liquid–hexatic–tetratic triple point.

which greatly broadens the spectrum of effective potentials possessing physical meaning (see, e.g., Refs [262–269]). From an applied standpoint, adjustable potentials offer broad possibilities for the 'self-assembly' of new materials [268, 270–273], which can be used in photonics, electronics, etc. [263].

The phase diagrams obtained using effective potentials may be qualitatively different from the case of standard molecular systems such as rare gases, whose phase diagram is known to be simple and adequately described by the well-known Lennard-Jones isotropic effective potentials. In this review, we discussed the behavior of systems with isotropic core-softened model potentials (with negative curvature in the repulsion region) in detail. These potentials can be used for the qualitative description of colloids, polymer globules, star-shaped polymers, and molecular systems, for instance water. It is shown that adding a repulsive step to the potential can radically change and complicate the form of the phase diagram: a variety of new crystal phases, maxima and minima in the melting curve, vitreous states, and anomalous beha-

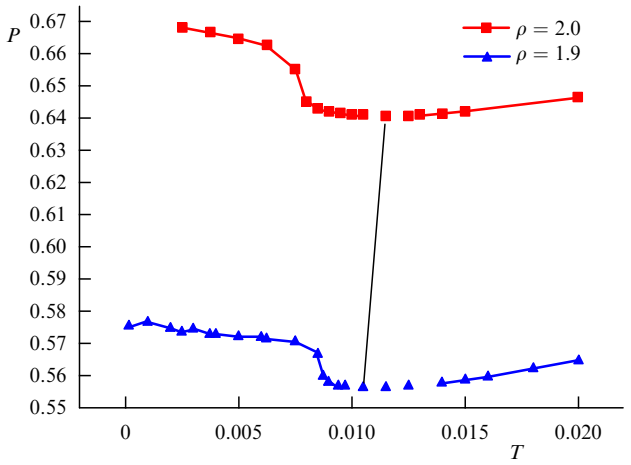

Figure 32. (Color online.) Isochores of Hertzian spheres on the right of the low-density triangular phase. The line connects the minima of the isochores.

viors in the liquid phase appear. This applies not only to the well-known water-like anomalies but also to other types of anomalies, for instance, to the anomalous behavior of liquid silica. Of special interest is the behavior of systems with core-softened potentials in the repulsion region as well as of systems with Hertzian finite potentials in the two-dimensional case. Manifested in the system in this case are not only diversified crystalline phases and liquid-phase anomalies, but also the amazing possibility of observing different melting scenarios in different domains of the phase diagram.

Therefore, it is safe to conclude that the use of isotropic effective potentials permits a qualitative (and in some cases, quantitative) description of the properties of the vast diversity of soft matter, especially when a microscopic ab initio study is impossible due to limited computing capabilities.

Acknowledgments

The authors express their appreciation to V V Brazhkin and D Frenkel for their interest in the work and fruitful discussions about different aspects of this review. The authors are also thankful to V V Brazhkin for critically reading the manuscript. Sections 1–4 and 6 were written with support from the Russian Science Foundation (grant no. 19-12-00092), and Section 5 was written with support from the Russian Foundation for Basic Research (grant no. 18-02-00981).

References

1. "60th anniversary of the Vereshchagin Institute for High Pressure Physics of the Russian Academy of Sciences (Scientific session of the Physical Sciences Division of the Russian Academy of Sciences, 25 April 2018)" *Phys. Usp.* **62** 198 (2019); "60 let Institutu fiziki vysokikh davlenii im. L F Vereshchagina RAN (Nauchnaya sessiya Otdeleniya fizicheskikh nauk Rossiiskoi akademii nauk, 25 aprelya 2018 g.)" *Usp. Fiz. Nauk* **189** 207 (2019)
2. Ekimov E A, Kondrin M V *Phys. Usp.* **62** 199 (2019); *Usp. Fiz. Nauk* **189** 208 (2019)
3. Filonenko V P et al. *Phys. Usp.* **62** 207 (2019); *Usp. Fiz. Nauk* **189** 217 (2019)
4. Alder B J, Wainwright T E *J. Chem. Phys.* **27** 1208 (1957)
5. Alder B J, Wainwright T E *J. Chem. Phys.* **31** 459 (1959)
6. Alder B J, Wainwright T E *J. Chem. Phys.* **33** 1439 (1960)
7. Alder B J, Wainwright T E *Phys. Rev.* **127** 359 (1962)
8. Balescu R *Equilibrium and Non-Equilibrium Statistical Mechanics* Vol. 1 (New York: Wiley, 1975); Translated into Russian: *Ravnovesnaya i Neravnovesnaya Statisticheskaya Mekhanika* Vol. 1 (Moscow: Mir, 1978)
9. Stishov S M *Sov. Phys. Usp.* **18** 625 (1975); *Usp. Fiz. Nauk* **114** 3 (1974)
10. Stishov S M *Fazovye Perekhody dlya Nachinayushchikh* (Phase Transitions for Beginners) 2nd ed. (Troitsk: Trovant, 2017)
11. Hansen J P, McDonald I R *Theory of Simple Liquids* 2nd ed. (London: Academic Press, 1986)
12. Hoover W G, Ree F H *J. Chem. Phys.* **47** 4873 (1967)
13. Stishov S M *Sov. Phys. Usp.* **31** 52 (1988); *Usp. Fiz. Nauk* **154** 93 (1988)
14. Barker J A, Henderson D *Rev. Mod. Phys.* **48** 587 (1976)
15. Ryzhov V N, Tareyeva E E *Phys. Lett. A* **75** 88 (1979)
16. Ryzhov V N, Tareeva E E *Theor. Math. Phys.* **48** 835 (1981); *Teor. Matem. Fiz.* **48** 416 (1981)
17. Ryzhov V N *Theor. Math. Phys.* **55** 399 (1983); *Teor. Matem. Fiz.* **55** 128 (1983)
18. Ashcroft N W, Lekner J *Phys. Rev.* **145** 83 (1966)
19. Fomin Yu D, Ryzhov V N, Brazhkin V V *J. Phys. Condens. Matter* **25** 285104 (2013)
20. Berlin T H, Montroll E W *J. Chem. Phys.* **20** 75 (1952)
21. Hoover W G, Gray S G, Johnson K W *J. Chem. Phys.* **55** 1128 (1971)
22. Zhakhovskii V V *JETP* **78** 871 (1994); *Zh. Eksp. Teor. Fiz.* **105** 1615 (1994)
23. Fomin Yu D, Brazhkin V V, Ryzhov V N *JETP Lett.* **95** 320 (2012); *Pis'ma Zh. Eksp. Teor. Fiz.* **95** 349 (2012)
24. Laird B B, Haymet A D J *Mol. Phys.* **75** 71 (1992)
25. Agrawal R, Kofke D A *Phys. Rev. Lett.* **74** 122 (1995)
26. Robbins M O, Kremer K, Grest G S *J. Chem. Phys.* **88** 3286 (1988)
27. Meijer E J, Frenkel D *J. Chem. Phys.* **94** 2269 (1991)
28. Hamaguchi S, Farouki R T, Dubin D H E *J. Chem. Phys.* **105** 7641 (1996)
29. Hamaguchi S, Farouki R T, Dubin D H E *Phys. Rev. E* **56** 4671 (1997)
30. Malescio G *J. Phys. Condens. Matter* **19** 073101 (2007)
31. Hagen M H J, Frenkel D *J. Chem. Phys.* **101** 4093 (1994)
32. Miller M A, Frenkel D *J. Chem. Phys.* **121** 535 (2004)
33. Liu H, Garde S, Kumar S *J. Chem. Phys.* **123** 174505 (2005)
34. Buckingham R A *Proc. R. Soc. Lond. A* **168** 264 (1938)
35. Ross M, McMahan A K *Phys. Rev. B* **21** 1658 (1980)
36. Belonoshko A B et al. *J. Chem. Phys.* **117** 7233 (2002)
37. Saija F, Prestipino S *Phys. Rev. B* **72** 024113 (2005)
38. Russel W B, Saville D A, Schowalter W R *Colloidal Dispersions* (Cambridge: Cambridge Univ. Press, 1989)
39. Meijer E J, Frenkel D *Phys. Rev. Lett.* **67** 1110 (1991)
40. Lekkerkerker H N W et al. *Europhys. Lett.* **20** 559 (1992)
41. Pusey P N et al. *J. Phys. Condens. Matter* **6** A29 (1994)
42. Calderon F L, Bibette J, Biais J *Europhys. Lett.* **23** 653 (1993)
43. Frenkel D *Science* **314** 768 (2006)
44. Girifalco L A *J. Phys. Chem.* **96** 858 (1992)
45. Hagen M H J et al. *Nature* **365** 425 (1993)
46. Cheng A, Klein M L, Caccamo C *Phys. Rev. Lett.* **71** 1200 (1993)
47. Hasegawa M, Ohno K *J. Phys. Condens. Matter* **9** 3361 (1997)
48. Costa D et al. *J. Chem. Phys.* **118** 304 (2003)
49. Xu L et al. *Proc. Natl. Acad. Sci. USA* **102** 16558 (2005)
50. Simeoni G G et al. *Nat. Phys.* **6** 503 (2010)
51. Gorelli F A et al. *Sci. Rep.* **3** 1203 (2013)
52. Gallo P, Corradini D, Rovere M *J. Chem. Phys.* **139** 204503 (2013)
53. Brazhkin V V, Ryzhov V N *J. Chem. Phys.* **135** 084503 (2011); *J. Chem. Phys.* **145** 059901 (2016)
54. Brazhkin V V et al. *J. Phys. Chem. B* **115** 14112 (2011)
55. Brazhkin V V et al. *Phys. Rev. E* **89** 042136 (2014)
56. Tareyeva E E, Ryzhov V N *Theor. Math. Phys.* **189** 1806 (2016); *Teor. Matem. Fiz.* **189** 464 (2016)
57. Fomin Yu D, Ryzhov V N, Tsiok E N, Brazhkin V V *Phys. Rev. E* **91** 022111 (2015)
58. Brazhkin V V *JETP Lett.* **95** 164 (2012); *Pis'ma Zh. Eksp. Teor. Fiz.* **95** 179 (2012)
59. Brazhkin V V et al. *Phys. Rev. E* **85** 031203 (2012)

60. Brazhkin V V et al. *Phys. Usp.* **55** 1061 (2012); *Usp. Fiz. Nauk* **182** 1137 (2012)
61. Brazhkin V V et al. *Phys. Rev. Lett.* **111** 145901 (2013)
62. Bolmatov D et al. *J. Chem. Phys.* **139** 234501 (2013)
63. Brazhkin V V et al. *Sverkhkriticheskie Flyuidy Teor. Praktika* **9** (2) 40 (2014)
64. Fomin Yu D et al. *Sci. Rep.* **4** 7194 (2014)
65. Fomin Yu D, Ryzhov V N, Tsiok E N, Brazhkin V V *Sci. Rep.* **5** 14234 (2015)
66. Fomin Yu D et al. *Physica A* **444** 890 (2016)
67. Gaiduk Eu A et al. *Fluid Phase Equilib.* **417** 237 (2016)
68. Fomin Yu D et al. *J. Phys. Condens. Matter* **28** 43LT01 (2016)
69. Fomin Yu D, Ryzhov V N, Tsiok E N, Brazhkin V V *J. Phys. Condens. Matter* **29** 345401 (2017)
70. Brazhkin V V et al. *J. Phys. Conf. Ser.* **950** 032019 (2017)
71. Fomin Yu D et al. *J. Phys. Condens. Matter* **30** 134003 (2018)
72. Brazhkin V V et al. *J. Phys. Chem. B* **122** 6124 (2018)
73. Brazhkin V V *Phys. Usp.* **60** 954 (2017); *Usp. Fiz. Nauk* **187** 1028 (2017)
74. Frenkel D *Science* **314** 768 (2006)
75. Tejero C F et al. *Phys. Rev. Lett.* **73** 752 (1994)
76. Daanoun A, Tejero C F, Baus M *Phys. Rev. E* **50** 2913 (1994)
77. Tejero C F et al. *Phys. Rev. E* **51** 558 (1995)
78. Bolhuis P, Frenkel D *Phys. Rev. Lett.* **72** 2211 (1994)
79. Tareyeva E E, Fomin Yu D, Tsiok E N, Ryzhov V N *Theor. Math. Phys.* **194** 148 (2018); *Teor. Matem. Fiz.* **194** 175 (2018)
80. Chaplin M "Anomalous properties of water", in Water Structure and Science, http://www.lsbu.ac.uk/water/anmlies.html
81. Brazhkin V V, Buldyrev S V, Ryzhov V N, Stanley H E (Eds) *New Kinds of Phase Transitions: Transforations in Disordered Substances* (Nato Science Series II, Vol. 81) (Dordrech: Kluwer Acad. Publ., 2002)
82. Tsuchiya Y *J. Phys. Condens. Matter* **3** 3163 (1991)
83. Thurn H, Ruska J *J. Non-Cryst. Solids* **22** 331 (1976)
84. Katayama Y et al. *J. Non-Cryst. Solids* **156 – 158** 687 (1993)
85. Sauer G E, Borst L B *Science* **158** 1567 (1967)
86. Kennedy S J, Wheeler J C *J. Chem. Phys.* **78** 1523 (1983)
87. Tsuchiya Y *J. Phys. Soc. Jpn.* **60** 227 (1991)
88. Gallo P et al. *Chem. Rev.* **116** 7463 (2016)
89. Angell C A et al. *Phys. Chem. Chem. Phys.* **2** 1559 (2000)
90. Sharma R, Chakraborty S N, Chakravarty C *J. Chem. Phys.* **125** 204501 (2006)
91. Shell M S, Debenedetti P G, Panagiotopoulos A Z *Phys. Rev. E* **66** 011202 (2002)
92. Poole P H, Hemmati M, Angell C A *Phys. Rev. Lett.* **79** 2281 (1997)
93. Sastry S, Angell C A *Nat. Mater.* **2** 739 (2003)
94. Vilaseca P, Franzese G *J. Non-Cryst. Solids* **357** 419 (2011)
95. Brazhkin V V, Voloshin R N, Popova S V *JETP Lett.* **50** 424 (1989); *Pis'ma Zh. Eksp. Teor. Fiz.* **50** 392 (1989)
96. Mishima O, Calvert L D, Whalley E *Nature* **314** 76 (1985)
97. Mishima O, Stanley H E *Nature* **396** 329 (1998)
98. Poole P H et al. *Nature* **360** 324 (1992)
99. Loerting T et al. *Phys. Chem. Chem. Phys.* **3** 5355 (2001)
100. Loerting T, Giovambattista N *J. Phys. Cond. Matter* **18** R19 (2006)
101. Tulk C A et al. *Phys. Rev. Lett.* **97** 115503 (2006)
102. Brazhkin V V et al. *High Pressure Res.* **15** 267 (1997)
103. Angell C A *Annu. Rev. Phys. Chem.* **55** 559 (2004)
104. Stanley H E et al. *AIP Conf. Proc.* **982** 251 (2008)
105. Liu L et al. *Phys. Rev. Lett.* **95** 117802 (2005)
106. Mallamace F et al. *Proc. Natl. Acad. Sci. USA* **105** 12725 (2008)
107. Cerveny S et al. *Chem. Rev.* **116** 7608 (2016)
108. Sheng H W et al. *Nat. Mater.* **6** 192 (2007)
109. Katayama Y et al. *Nature* **403** 170 (2000)
110. Monaco G et al. *Phys. Rev. Lett.* **90** 255701 (2003)
111. Katayama Y et al. *Science* **306** 848 (2004)
112. Henry L et al., arXiv:1709.09996
113. Hemmer P C, Stell D *Phys. Rev. Lett.* **24** 1284 (1970)
114. Stell G, Hemmer P C *J. Chem. Phys.* **56** 4274 (1972)
115. Young D A, Alder B J *Phys. Rev. Lett.* **38** 1213 (1977)
116. Stishov S M *Phil. Mag. B* **82** 1287 (2002)
117. Ryzhov V N, Stishov S M *JETP* **95** 710 (2002); *Zh. Eksp. Teor. Fiz.* **122** 820 (2002)
118. Ryzhov V N, Stishov S M *Phys. Rev. E* **67** 010201(R) (2003)
119. Fomin Yu D, Ryzhov V N, Tareyeva E E *Phys. Rev. E* **74** 041201 (2006)
120. Hoover W G, Gray S G, Johnson K W *J. Chem. Phys.* **55** 1128 (1971)
121. Dotera T, Oshiro T, Ziherl P *Nature* **506** 208 (2014)
122. Pattabhiramana H, Dijkstra M *J. Chem. Phys.* **146** 114901 (2017)
123. Pattabhiramana H, Dijkstra M *Soft Matter* **13** 4418 (2017)
124. Franzese G et al. *Nature* **409** 692 (2001)
125. Franzese G et al. *Phys. Rev. E* **66** 051206 (2002)
126. Sadr-Lahijany M R et al. *Phys. Rev. Lett.* **81** 4895 (1998)
127. Sadr-Lahijany M R et al. *Phys. Rev. E* **60** 6714 (1999)
128. Malescio G, Pellicane G *Phys. Rev. E* **63** 020501(R) (2001)
129. Jagla E A *J. Chem. Phys.* **111** 8980 (1999)
130. Jagla E A *Phys. Rev. E* **63** 061501 (2001)
131. de Oliveira A B et al. *J. Chem. Phys.* **124** 084505 (2006)
132. Franzese G *J. Mol. Liq.* **136** 267 (2007)
133. Vilaseca P, Franzese G *J. Chem. Phys.* **133** 084507 (2010)
134. Vilaseca P, Franzese G *J. Non-Cryst. Solids* **357** 419 (2011)
135. Buldyrev S V et al. *J. Phys. Condens. Matter* **21** 504106 (2009)
136. de Oliveira A B et al. *J. Chem. Phys.* **128** 064901 (2008)
137. Leoni F, Franzese G *J. Chem. Phys.* **141** 174501 (2014)
138. Likos C N *Soft Matter* **2** 478 (2006)
139. Athanasopoulou L, Ziherl P *Soft Matter* **13** 1463 (2017)
140. Pàmies J C, Cacciuto A, Frenkel D *J. Chem. Phys.* **131** 044514 (2009)
141. Stillinger F H *J. Chem. Phys.* **65** 3968 (1976)
142. Stillinger F H, Weber T A *Phys. Rev. B* **22** 3790 (1980)
143. Ahmed A, Mausbach P, Sadus R J *J. Chem. Phys.* **131** 224511 (2009)
144. Ahmed A, Mausbach P, Sadus R J *Phys. Rev. E* **82** 011201 (2010)
145. Mausbach P, Sadus R J *J. Chem. Phys.* **134** 114515 (2011)
146. Shvab I, Sadus R J *Fluid Phase Equilib.* **407** 7 (2016)
147. Prestipino S, Saija F, Giaquinta P V *Phys. Rev. E* **71** 050102(R) (2005)
148. Prestipino S et al. *J. Chem. Phys.* **140** 084906 (2014)
149. Losey J, Sadus R J *Phys. Rev. E* **100** 012112 (2019)
150. Debenedetti P G, Raghavan V S, Borick S S *J. Phys. Chem.* **95** 4540 (1991)
151. Sperl M et al. *Phys. Rev. Lett.* **104** 145701 (2010)
152. Ryzhov V N, Tareyeva E E, Fomin Yu D *Theor. Math. Phys.* **167** 645 (2011); *Teor. Matem. Fiz.* **167** 284 (2011)
153. Ryzhov V N, Tareyeva E E *Phys. Lett. A* **378** 3567 (2014)
154. Fomin Yu D et al. *J. Chem. Phys.* **129** 064512 (2008)
155. Fomin Yu D, Gribova N V, Ryzhov V N *Defect Diffus. Forum* **277** 155 (2008)
156. Gribova N V, Fomin Yu D, Frenkel D, Ryzhov V N *Phys. Rev. E* **79** 051202 (2009)
157. Fomin Yu D, Tsiok E N, Ryzhov V N *J. Chem. Phys.* **134** 044523 (2011)
158. Fomin Yu D, Ryzhov V N, Gribova N V *Phys. Rev. E* **81** 061201 (2010)
159. Abraham J Y, Buldyrev S V, Giovambattista N *J. Phys. Chem. B* **115** 14229 (2011)
160. Higuchi S et al. *J. Chem. Phys.* **148** 094507 (2018)
161. Frenkel D, Smit B *Understanding Molecular Simulation: from Algorithms to Applications* 2nd ed. (New York: Academic Press, 2002)
162. Stanley H E *Introduction to Phase Transitions and Critical Phenomena* (Oxford: Clarendon Press, 1971)
163. Kofke D A, Bolhuis P G *Phys. Rev. E* **59** 618 (1999)
164. Rascón C et al. *J. Chem. Phys.* **106** 6689 (1997)
165. Binder K, Kob W *Glassy Materials and Disordered Solids: An Introduction to Their Statistical Mechanics* (Singapore: World Scientific, 2005)
166. Götze W *Complex Dynamics of Glass-Forming Liquids: a Mode-Coupling Theory* (Oxford: Oxford Univ. Press, 2009)
167. Ryltsev R E, Chtchelkatchev N M, Ryzhov V N *Phys. Rev. Lett.* **110** 025701 (2013)
168. Ryltsev R E, Chtchelkatchev N *Soft Matter* **13** 5076 (2017)
169. Chaplin M "Water phase diagram", in Water Structure and Science, http://www1.lsbu.ac.uk/water/water_phase_diagram.html
170. Kob W, Andersen H C *Phys. Rev. Lett.* **73** 1376 (1994)
171. Wahnström G *Phys. Rev. A* **44** 3752 (1991)
172. Toxvaerd S et al. *J. Chem. Phys.* **130** 224501 (2009)

173. Pedersen U R et al., arXiv:0706.0813
174. Fomin Yu D, Ryzhov V N, Klumov B A, Tsiok E N *J. Chem. Phys.* **141** 034508 (2014)
175. Lowe C P *Europhys. Lett.* **47** 145 (1999)
176. Koopman E A, Lowe C P *J. Chem. Phys.* **124** 204103 (2006)
177. Truskett T M, Torquato S, Debenedetti P G *Phys. Rev. E* **62** 993 (2000)
178. Errington J R, Debenedetti P G *Nature* **409** 318 (2001)
179. Errington J R, Truskett Th M, Mittal J *J. Chem. Phys.* **125** 244502 (2006)
180. de Oliveira A B et al. *J. Chem. Phys.* **132** 234509 (2010)
181. Fomin Yu D *Phys. Chem. Liq.* **57** 67 (2019)
182. Fomin Yu D *Mol. Phys.* **117** 2786 (2019)
183. de Oliveira A B, Netz P A, Barbosa M C *Europhys. Lett.* **85** 36001 (2009)
184. Fomin Yu D, Tsiok E N, Ryzhov V N *J. Chem. Phys.* **135** 234502 (2011)
185. Fomin Yu D, Tsiok E N, Ryzhov V N *Eur. Phys. J. Spec. Top.* **216** 165 (2013)
186. Fomin Yu D, Ryzhov V N *Phys. Lett. A* **375** 2181 (2011)
187. Fomin Yu D, Tsiok E N, Ryzhov V N *J. Chem. Phys.* **135** 124512 (2011)
188. Fomin Yu D, Ryzhov V N *Adv. Chem. Phys.* **152** 81 (2013)
189. Fomin Yu D, Tsiok E N, Ryzhov V N *Phys. Rev. E* **87** 042122 (2013)
190. Fomin Yu D, Ryzhov V N *Phys. Lett. A* **377** 1469 (2013)
191. Ryzhov V N, Tareyeva E E, Fomin Yu D, Tsiok E N *Phys. Usp.* **60** 857 (2017); *Usp. Fiz. Nauk* **187** 921 (2017)
192. Ryzhov V N *Phys. Usp.* **60** 114 (2017); *Usp. Fiz. Nauk* **187** 125 (2017)
193. Kosterlitz J M *Rep. Prog. Phys.* **79** 026001 (2016)
194. Kosterlitz J M *Rev. Mod. Phys.* **89** 040501 (2017)
195. Landau L D *Phys. Z. Sowjetunion* **11** 26 (1937)
196. Peierls R E *Helv. Phys. Acta* **7** 81 (1934)
197. Peierls R E *Ann. Inst. Henri Poincaré* **5** 177 (1935)
198. Bogolubov N N (Jr.) "Quasi-averages in problems of statistical mechanics" *Quantum Statistical Mechanics: Selected Works* (Hackensack, NJ: World Scientific, 2015); Translated from Russian: "Kvazisrednie v zadachakh statisticheskoi mekhaniki", in *Sobranie Nauchnykh Trudov v Dvenadtsati Tomakh* Vol. 6 (Moscow: Nauka, 2006) p. 236
199. Sadovnikov B I, Fedyanin V K *Theor. Math. Phys.* **16** 901 (1973); *Teor. Matem. Fiz.* **16** 368 (1973)
200. Sadovnikov B I, Sorokina E M *Sov. Phys. Dokl.* **14** 968 (1970); *Dokl. Akad. Nauk SSSR* **188** 788 (1969)
201. Mermin N, Wagner H *Phys. Rev. Lett.* **17** 1133 (1966)
202. Mermin N, Wagner H *Phys. Rev.* **17** 1307 (1966)
203. Mermin N D *Phys. Rev.* **176** 250 (1968)
204. Berezinskii V L *Sov. Phys. JETP* **32** 493 (1971); *Zh. Eksp. Teor. Fiz.* **59** 907 (1970)
205. Berezinskii V L *Sov. Phys. JETP* **34** 610 (1972); *Zh. Eksp. Teor. Fiz.* **61** 1144 (1971)
206. Kosterlitz J M, Thouless D J *J. Phys. C* **6** 1181 (1973)
207. Kosterlitz J M, Thouless D J *J. Phys. C* **5** L124 (1972)
208. Halperin B I, Nelson D R *Phys. Rev. Lett.* **41** 121 (1978)
209. Nelson D R, Halperin B I *Phys. Rev. B* **19** 2457 (1979)
210. Young A P *Phys. Rev. B* **19** 1855 (1979)
211. Gasser U et al. *Chem. Phys. Phys. Chem.* **11** 963 (2010)
212. Keim P, Maret G, von Grünberg H H *Phys. Rev. E* **75** 031402 (2007)
213. Dillmann P, Maret G, Keim P *J. Phys. Condens. Matter* **20** 404216 (2008)
214. Assoud L et al. *Phys. Rev. Lett.* **102** 238301 (2009)
215. Deutschländer S et al. *Phys. Rev. Lett.* **113** 127801 (2014)
216. Kapfer S C, Krauth W *Phys. Rev. Lett.* **114** 035702 (2015)
217. Chui S T *Phys. Rev. B* **28** 178 (1983)
218. Chui S T *Phys. Rev. Lett.* **48** 933 (1982)
219. Kleinert H *Phys. Lett. A* **95** 381 (1983)
220. Kleinert H *Phys. Lett. A* **96** 302 (1983)
221. Ryzhov V N *Sov. Phys. JETP* **73** 899 (1991); *Zh. Eksp. Teor. Fiz.* **100** 1627 (1991)
222. Ryzhov V N *Theor. Math. Phys.* **88** 990 (1991); *Teor. Matem. Fiz.* **88** 449 (1991)
223. Ryzhov V N, Tareeva E E *Theor. Math. Phys.* **92** 922 (1992); *Teor. Matem. Fiz.* **92** 331 (1992)
224. Ryzhov V N *J. Phys Condens. Matter* **2** 5855 (1990)
225. Ryzhov V N, Tareyeva E E *Phys. Rev. B* **51** 8789 (1995)
226. Ryzhov V N, Tareeva E E *JETP* **81** 1115 (1995); *Zh. Eksp. Teor. Fiz.* **108** 2044 (1995)
227. Ryzhov V N, Tareyeva E E *Physica A* **314** 396 (2002)
228. Ryzhov V N, Tareyeva E E *Theor. Math. Phys.* **130** 101 (2002); *Teor. Matem. Fiz.* **130** 119 (2002)
229. Chumakov E S et al. *Physica A* **432** 279 (2015)
230. Ryzhov V N et al. *Theor. Math. Phys.* **191** 842 (2017); *Teor. Matem. Fiz.* **191** 424 (2017)
231. Ryzhov V N, Tareyeva E E *Phys. Lett. A* **75** 88 (1979)
232. Bernard E P, Krauth W *Phys. Rev. Lett.* **107** 155704 (2011)
233. Engel M et al. *Phys. Rev. E* **87** 042134 (2013)
234. Qi W, Gantapara A P, Dijkstra M *Soft Matter* **10** 5449 (2014)
235. Tsiok E N, Fomin Y D, Ryzhov V N *Physica A* **490** 819 (2018)
236. Thorneywork A L et al. *Phys. Rev. Lett.* **118** 158001 (2017)
237. Minnhagen P *Rev. Mod. Phys.* **59** 1001 (1987)
238. Minnhagen P, Wallin M *Phys. Rev. B* **36** 5620 (1987)
239. Jonsson A, Minnhagen P, Nylén M *Phys. Rev. Lett.* **70** 1327 (1993)
240. Levin Y, Li X, Fisher M E *Phys. Rev. Lett.* **73** 2716 (1994)
241. Ryzhov V N, Tareyeva E E *Phys. Rev. B* **48** 12907 (1993)
242. Ryzhov V N, Tareyeva E E *Phys. Rev. B* **49** 6162 (1994)
243. Irz D Yu, Ryzhov V N, Tareeva E E *Theor. Math. Phys.* **107** 499 (1996); *Teor. Matem. Fiz.* **107** 100 (1996)
244. Irz D Yu, Ryzhov V N, Tareyeva E E *Phys. Rev. B* **54** 3051 (1996)
245. Algara-Siller G et al. *Nature* **519** 443 (2015)
246. Zhao J et al. *Science* **343** 1228 (2014)
247. Tsiok E N, Dudalov D E, Fomin Yu D, Ryzhov V N *Phys. Rev. E* **92** 032110 (2015)
248. Dudalov D E, Fomin Yu D, Tsiok E N, Ryzhov V N *J. Phys. Conf. Ser.* **510** 012016 (2014)
249. Dudalov D E, Fomin Yu D, Tsiok E N, Ryzhov V N *J. Chem. Phys.* **141** 18C522 (2014)
250. Dudalov D E, Fomin Y D, Tsiok E N, Ryzhov V N *Soft Matter* **10** 4966 (2014)
251. Kryuchkov N P et al. *Soft Matter* **14** 2152 (2018)
252. Fomin Yu D, Gaiduk E A, Tsiok E N, Ryzhov V N *Mol. Phys.* **116** 3258 (2018)
253. Tsiok E N, Gaiduk E A, Fomin Yu D, Ryzhov V N, arXiv:1911.06086
254. LAMMPS Molecular Dynamics Simulator, http://lammps.sandia.gov/
255. Mayer J E, Wood W W *J. Chem. Phys.* **42** 4268 (1965)
256. Krebs Z et al. *J. Chem. Phys.* **149** 034503 (2018)
257. Landau L D, Lifshitz E M *Theory of Elasticity* (Oxford: Pergamon Press, 1986); Translated from Russian: *Teoriya Uprugosti* (Moscow: Fizmatlit, 2001)
258. Pàmies J C, Cacciuto A, Frenkel D *J. Chem. Phys.* **131** 044514 (2009)
259. Miller W L, Cacciuto A *Soft Matter* **7** 7552 (2011)
260. Zu M, Tan P, Xu N *Nat. Commun.* **8** 2089 (2017)
261. Zu M et al. *Phys. Rev. Lett.* **117** 085702 (2016)
262. Ivlev A et al. *Complex Plasmas and Colloidal Dispersions: Particle-Resolved Studies of Classical Liquids and Solids* (Series in Soft Condensed Matter, Vol. 5) (Singapore: Word Scientific, 2012)
263. Fernandez-Nieves A, Puertas A M (Eds) *Fluids, Colloids, and Soft Materials: an Introduction to Soft Matter Physics* (New York: Wiley, 2016)
264. Fortov V E et al. *Phys. Usp.* **47** 447 (2004); *Usp. Fiz. Nauk* **174** 495 (2004)
265. Fortov V E *Phys. Usp.* **50** 333 (2007); *Usp. Fiz. Nauk* **177** 347 (2007)
266. Klumov B A *Phys. Usp.* **53** 1053 (2010); *Usp. Fiz. Nauk* **180** 1095 (2010)
267. Tsytovich V N *Phys. Usp.* **58** 150 (2015); *Usp. Fiz. Nauk* **185** 161 (2015)
268. Couëdel L et al. *Phys. Usp.* **62** 1000 (2019); *Usp. Fiz. Nauk* **189** 1070 (2019)
269. Kryuchkov N P, Khrapak S A, Yurchenko S O *J. Chem. Phys.* **146** 134702 (2017)
270. Tang X et al. *ACS Nano* **10** 6791 (2016)
271. Zaytsev K I, Yurchenko S O *Appl. Phys. Lett.* **105** 051902 (2014)
272. Zaytsev K I et al. *J. Appl. Phys.* **115** 213505 (2014)
273. Yurchenko S O et al. *J. Phys. D* **50** 055105 (2017)